2013

Characterization of Polyetherimide Under Static, Dynamic, and Multiple Impact Conditions

Bryan Zuanetti
University of Central Florida

CHARACTERIZATION OF POLYETHERIMIDE UNDER STATIC, DYNAMIC, AND MULTIPLE IMPACT CONDITIONS

by

BRYAN ZUANETTI

A thesis submitted in partial fulfillment of the requirements
for the Honors in the Major Program in Mechanical Engineering
in the College of Engineering and Computer Sciences
and in The Burnett Honors College
at the University of Central Florida
Orlando, Florida

Fall Term 2013

Thesis Chair: Dr. Ali P. Gordon

ABSTRACT

The application of polymers in robust engineering designs is on the rise due to their excellent mechanical properties such as high fracture toughness, specific strength, durability, as well as, thermal and chemical resistances. Implementation of some advanced polymeric solids is limited due to the lack of available mechanical properties. In order for these materials to endure strenuous engineering designs it is vital to investigate their response in multiple loading rates and conditions. In this thesis, the mechanical response of polyethermide (PEI) is characterized under quasi-static, high strain rate, and multiple impact conditions. Standard tension, torsion, and compression experiments are performed in order to distinguish the multi-regime response of PEI. The effects of physical ageing and rejuvenation on the quasi-static mechanical response are investigated. The strain softening regime resulting from strain localization is eliminated by thermal and mechanical rejuvenation, and the advantages of these processes are discussed. The dynamic fracture toughness of the material in response to notched impact via Charpy impact test is evaluated. The high strain-rate response of PEI to uniaxial compression is evaluated at rates exceeding 10^4/s via miniaturized Split Hopkinson Pressure Bar (MSHPB), and compared to the quasi-static case to determine strain-rate sensitivity. The elastic response of the aged material to multiple loading conditions are correlated using the Ramberg-Osgood equation, while the elastoplastic response of rejuvenated PEI is correlated using a both the Ramberg-Osgood equation and a novel model. The strain-rate sensitivity of the strength is found to be nominally bilinear and transition strains are modeled using the Ree-Erying formulation. Finally, multiple impact experiments are performed on PEI using the MSHPB and a model is proposed to quantify damage as a result of collision.

ACKNOWLEDGMENTS

I would like to express my very great appreciation to my committee members whose valuable support was vital for the completion of this investigation. First, I would like to express my deep gratitude for my thesis chair, and advisor, Dr. Ali P. Gordon, whose valuable and constructive suggestions were critical for my professional growth throughout my undergraduate career. Next, I would like to thank Dr. Seetha Raghavan for support, and for providing meaningful experiences which shaped the course of my research. I would like to thank Dr. Cheryl Xu who served not only as part of my committee, but as my technical advisor, and whose support facilitated the completion of many challenging research complications. I am also very thankful to Dr. George Sunny whose knowledgeable advice has greatly strengthened my understanding of research and experimental design.

Next, I would like to thank several individuals whom have assisted me with various aspects of this investigation. I would like to extend a special thanks to Nathan Mutter whom first introduced me to this topic, and provided key explanations in order for me to begin my research. Nathan stood by me as I ran all the experiments in the initial phase of this investigation, and provided research articles that served as the backbone of my literature review. Kevin Smith advised me with technical details for computer simulations. Allan Owiji expertly photographed the fracture surfaces of my tensile and Impact samples. Charles Mansfield performed torsion experiments with the help of several students from the solid mechanics lab. Finally, I would like to thank my family for encouragement throughout my years of undergraduate research.

TABLE OF CONTENTS

LIST OF FIGURES

LIST OF TABLES

1. INTRODUCTION

The development of new technologies has increased the challenges of service conditions that mechanical components undergo. As these service conditions become increasingly more strenuous there is a greater need for the development of durable designs which incorporate strong and heavy-duty materials. Developing these materials can prove to be difficult, but characterizing them is a task on its own. In the past years, the application of polymeric solids for robust engineering designs has greatly increased. These materials are sought after due to their excellent mechanical properties such as fracture toughness, specific strength, durability, as well as, thermal and chemical resistances. However, the implementation of many of these advanced polymeric solids can be limited due to the lack of available mechanical properties. This issue becomes increasingly more significant considering the established dependency of polymers to an increase in temperature, and deformation rates. To address the need for durable polymeric designs, it is vital to characterize these materials in both static and dynamic conditions. Recently, thermoplastics such as polycarbonate (PC), polypropylene (PP), and polyetheretherketone (PEEK) have been implemented in various mechanical designs. These thermoplastics are advantageous due to their ability to be reformed, and thus recyclable. A thermoplastic that has been used in various structural and dynamic engineering applications, but has not been fully characterized is polyetherimide (PEI). This material has experienced use in various applications due to its excellent mechanical strength and favorable characteristics as opposed to other thermoplastics. In the present study, the mechanical response of PEI is investigated under quasi-static and high strain rate conditions. In the quasi-static case, standard tension, torsion, and compression experiments are performed on PEI. Ageing, an effect resulting in strain

localizations that cripple the ductility and toughness of the material are investigated, and methods to eliminate such processes are discussed. The response of PEI to uniaxial high strain-rate compression is evaluated by means of a miniature Split Hopkinson Pressure Bar (mSHPB), and the rate sensitivity of the material is discussed. The elastoplastic response of PEI to quasi-static deformation for several cases, and the rate sensitivity of the material are modeled. Finally, multiple impact experiments are performed on PEI and the results are discussed. This thesis is intended to confirm and expand the knowledge of the properties of PEI for future innovative applications.

A review of literature regarding the material response, and techniques utilized to analyze such responses are proposed in Chapter 2. The experimental setup and procedures used to evaluate the response of PEI to quasi-static and high strain-rate deformation are discussed in chapter 3 and 4, respectively. The results for these experiments are presented and modeled in chapter 5 and 6, respectively. Finally, the discussion of results, and plan for future work, as well as, references, data and codes are provided in chapter 7 and 8, respectively.

2. BACKGROUND

2.1 Material Background

2.1.1 Polyetherimide (Ultem 1000)

Unreinforced PEI, commonly referred to as Ultem 1000 is an advanced amorphous thermoplastic developed by General Electric Co. with superb thermal, electrical and mechanical properties. PEI is the result of combining units of ether and aromatic imides leading to the large monomer $C_{37}H_{24}O_6N_{27}$. The chemical composition and molecular structure of PEI is shown in Fig 1. It is known that ether units supply the excellent flow and flexibility to the melt, while imide units provide excellent mechanical and thermal resistances (Chen e. a., 2006). This polymer is commonly synthesized via polycondensation of dianhydride 4,4', with m-phenylene diamine. This material is both x-ray amorphous (i.e., the polymer chains lack long range order) and exhibits a glass transition, thus being categorized as a glassy polymer. The favorable characteristics of PEI have led to its use in various industrial applications. This material has been used in injection molding of a variety of interior and structural components in the Fokker 50 and 100 series aircraft [Beland, 2009]. It has been used for thermostat housing, transmission components, and throttle bodies in automobiles [Bierogel, et al 2008]. In addition, PEI has been used to manufacture sterilization trays and surgical probes for the medical industry [Swallowe, 1999].

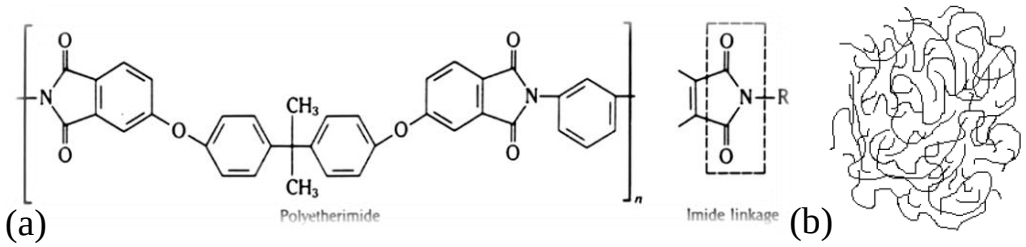

Figure 1. (a) Molecular arrangement, and (b) amorphous polymer chain of Ultem 1000.

2.1.2 Previously Characterized Properties

Because polyetherimide has been used in various industrial applications some of its properties have been previously investigated, such as in tribological, structural, and impact applications. A variety of researchers have also developed the mechanical properties of PEI and select properties are provided in table 1. Polytetrafluroethylene (PTFE) has been shown to decrease the frictional coefficient of PEI, and glass-fibre reinforcement has been shown to increase wear resistance at a tradeoff for ductility [Bijwe, 1990]. Facca showed that it was possible to predict the linear elastic behavior of the material from thermodynamic processes [Facca, 2006], and the properties of carbon fibre reinforced PEI were evaluated via Izod Impact Experiment [Smmazcelik, 2008]. Researchers have also investigated novel production processes to increase the properties of PEI in specific applications, such as the addition of alumina or silica nano-particles which increase the ultimate strength of PEI, or the fabrication of nanofoams with higher specific modulus and thermal resistances than other foams [Chen, 2006; Bansal, 2002; Zhou, 2012].

In the quasi-static case, the mechanical response of PEI is similar to that of other amorphous thermoplastics, in such a way that it is marked by four distinctive mechanical regimes before rupturing: (1) linear elastic, (2) non-linear elastic, (3) strain softening, and (4) strain hardening. The response of PEI to quasi-static compression is shown in Fig 2. Initially, PEI responds linearly to stress, this response is dictated by the van der waal forces present during the interaction between polymer chains as they slide with respect to one another. As deformation continues, the stress in localized areas of the material increase to a level by which they overcome

the van der waal forces, at this point the response becomes notably non-linear. The non-linear response continues until high stresses propagate throughout the sample and the material yields, for amorphous polymers the yield strength is denoted as the local maximum stress prior to strain softening. The third mechanical regime has been a source of some debate, of whether it is characterized by a local temperature rise [Marshall, 1954], or a permanent rearrangement of polymer chains [Brown, 1968; Vincent, 1960], but the latter has been accepted. It is known that amorphous polymers exist in a state of non-equilibrium, and with enough time theoretically mobilize to a lower energy state. The rate at which they mobilize is directly related to the ratio of the temperature application and their glass transition temperature. This phenomenon has been extensively researched and shown to increase free volume at the expense of mobility within the material. This process referred to as physical ageing in polymers promotes strain localizations which can cripple the ductility of the material during the strain softening regime [Struik, 1978; Simon, 1996; Garcia, 2007; Mahajan, 2010; Marano, 2013]. Subsequent to strain softening, the material begins to harden in response to an alignment of once randomly oriented polymer chains in a way where increased stress is required for continued flow, and finally the material ruptures.

Despite the limited available mechanical data the quasi-static properties of PEI are relatively well understood, however, most investigations focused on a single mode of mechanical response. Further research is needed to improve the confidence of designs in multi-modal applications. Furthermore, the response of PEI to high deformation rates has received even less attention, and these investigations are vital given the polymeric sensitivity to high rates of deformation. To further understand the response of polymers the following section will discuss the background of previous polymer high strain-rate investigations.

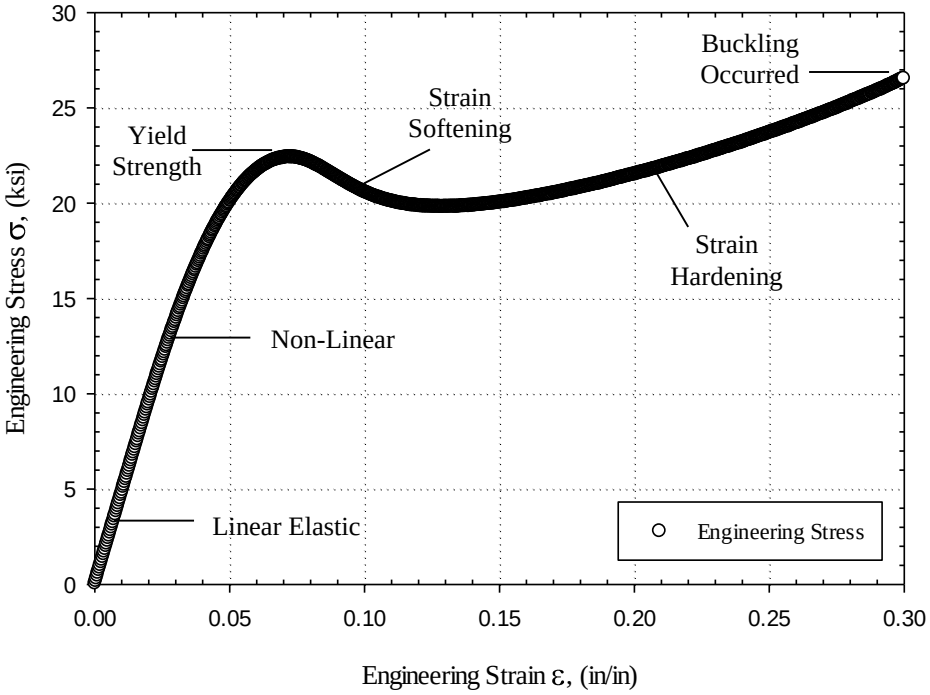

Figure 2. Response of PEI to quasi-static uniaxial compression.

Table 1. Mechanical and thermal properties of Ultem 1000 [Mutter, 2010].

Mechanical Properties	**Value (English)**	**Value (SI)**
Tensile Modulus, E_t	475 ksi	3.28 GPa
Compressive Modulus, E_c	480 ksi	3.31 GPa
Flexural Modulus, E_f	500 ksi	3.45 GPa
Poisson's Ratio, ν	0.36	0.36
Elongation (Yield), ε_y	7.0 %	7.0 %
Tensile Strength, σ_{ut}	16.5 ksi	113.8 MPa
Compressive Strength, σ_{uc}	22 ksi	151.7 MPa
Shear Strength, σ_{su}	15 ksi	103.4 MPa
Flexural Strength, σ_{uf}	20 ksi	137.9 MPa
Elongation (Fracture), ε_f	60 %	60 %
Izod Impact Resistance, Notched	1.0 ft-lbs/in	0.034 J/m
Rockwell Hardness, HRM	109	109
Physical Properties	**Value (English)**	**Value (SI)**
Specific Gravity	1.28	1.28
Thermal Properties	**Value (English)**	**Value (SI)**
CTE-Flow, α_f	31 μin/in-°F	55.8 μm/m-°C
Glass Temperature, T_g	419°F	215°C

2.1.3 High Rate Polymer Investigations

It is a well-known phenomenon that materials exhibit and increase in strength in response to increasing strain-rates. The same has been found when investigating the dynamic response of polymeric solids. Chou et al. employed a custom medium strain-rate machine and a Kolsky bar apparatus to study the response of polymethylmethacrylate PMMA, cellulose acetate butyrate (CAB), polypropylene (PP), and nylon 6 to a wide range of strain rates. It was noted that a positively sloped relationship existed between the strength of the polymers and the rate at which they were deformed [Chou, 1973]. Similar investigations were performed on a range of polymers by Walley and Field [Walley, 1989; Walley, 1991; Field, 1994]. They too noted a positively sloped strain rate dependency in the yield strength of the polymers, and went further to classify this relationship into three groups. The first is a positively sloped linear relationship, followed by a positively sloped bilinear relationship, while the final is a decrease in the strength of the material at approximately 10^3/s strain rate. The stress-strain response and rate dependency of polycarbonate PC found in an investigation by Sivour, is illustrated in Fig 3 and Fig 4 [Sivour, 2005].

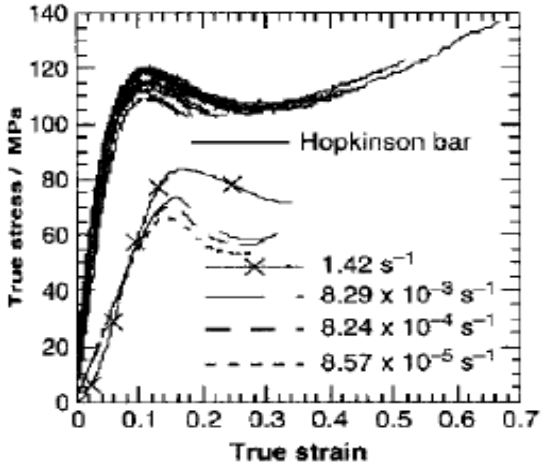

Figure 3. Stress-strain response of PC for multiple strain rates [Sivour, 2005].

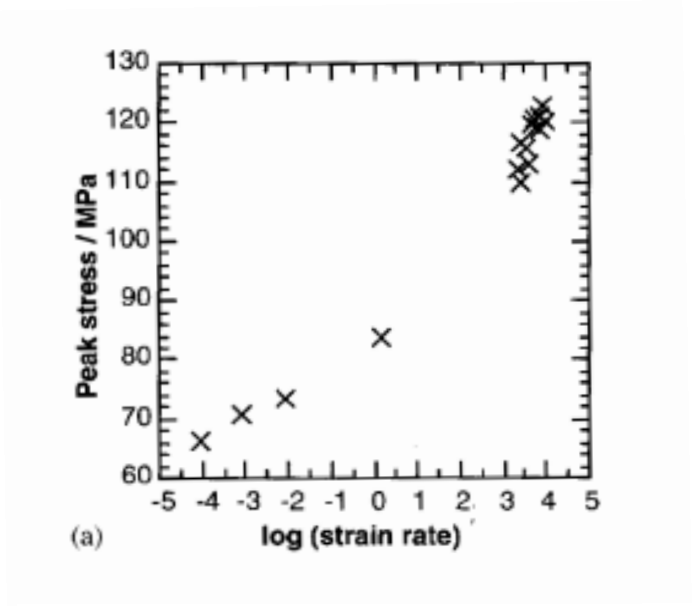

Figure 4. Rate sensitivity of PC strength [Siviour, 2005].

As shown above the rate sensitivity of amorphous polymers is vital to the understanding of the mechanical response, and for each rate sensitivity group it is necessary to model this behavior. In order to model the linear rate dependency of the yield strength in amorphous polymers the Eyring activation theory [Eyring, 1936] has been used by researchers, but for materials which exhibit a bilinear behavior, a modified version of the Eyring activation theory, knows as the Ree-Erying model [Ree, 1955] has been developed and utilized [Roetling, 1965]. The techniques stated above will be used in the following investigation to study the behavior of PEI, further information detailing the models will be presented in chapter 7. In the following section the history of the Split Hopkinson Pressure Bar will be provided, as well as, a background detailing the theory and assumptions required for acquiring the stress-strain response of materials at high deformation rates.

2.2 Split Hopkinson Pressure Bar Background

2.2.1 History

The Hopkinson Pressure Bar (HPB) was developed by Bertram Hopkinson as a means of generating pressure waves associated with dynamic conditions. Although Hopkinson developed the device to study the behavior of waves as the propagated through cylindrical mediums [Hopkinson, 1914], Davies and Kolsky further developed the device in order to attain a constitutive response of a material under high deformation rates [Davies, 1948; Kolsky, 1949]. The new device was called the "Split Hopkinson Pressure Bar" (SHPB) or simply Kolsky bar, because the original bar was divided into two bars in order to contain a sample. Since the development of the SHPB, the technique has been modified in order to load materials in multi-modes, such as tension, torsion, shear, biaxial, and triaxial modes [Harding, 1960; Nicholas, 1981; Staab, 1991, Gilat, 2000; Nemat, 2000]. Further, modifications have been made for precise control of the apparatus such as pulse shaping and momentum trapping, which are critical for steady strain-rates, and dynamic recovery experiments, respectively.

The SHPB is not a commercially available device nor does it possess an ASTM standard, however, guidelines due exist which detail the design, experimental analysis, and solutions to various experimental complications [Gray, 2000; Chen, 2011; Mutter, 2011]. Special considerations are required when using the SHPB technique to test varying materials. Modifications have been made to the technique in order to test ceramics [Zhao, 1998; Subhash, 2000], low impedance materials [Blumenthal, 2000], and even metallic glasses [Sunny, 2012]. Mathematical techniques to correct error in the acquired pulses due to wave dispersion have been

developed by various researchers [Follanbee, 1983; Gong, 1990; Gorham, 1983; Lifshitz, 1994; Tyas, 2005]. High resolution optical strain measurement techniques have been studied to correct similar effects [Siviour, 2009; Ramesh, 2007; Swantek, 2011], and the minituarized Split Hopkinson Pressure Bar (mSHPB) has been rigorously studied [Jia and Ramesh, 2004]. This technique has been shown to possess advantages over the full scale setup, such as an increase in the strain-rate limit, a reduction of the negative effects from wave dispersion, friction and inertia.

2.2.2 SHPB Theory

Now that the history of the apparatus has been discussed, a brief review of the SHPB theory will be discussed in this section. Further details and derivations can be found in the ASM handbook [Gray, 2004]. In application, pressures waves transverse a slender bar and impart a dynamic load to an adjacent specimen. Because these devices can generate strain rates on the order of 10^5/s it is reasonable that conditions similar to explosive detonations or bullet impact can be simulated in a lab type environment. The classic SHPB had three main components; the striker bar, the impact bar, and the transmission bar. An illustration of the classic setup is shown in Fig 5.

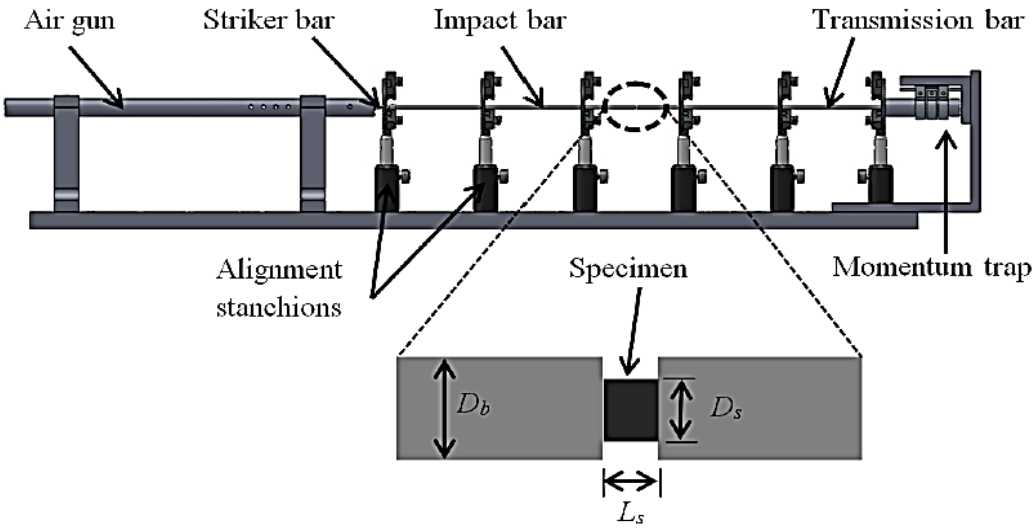

Figure 5. Classic Split Hopkinson Pressure Bar Apparatus.

Under compression, a sample located between the incident and transmission bars is compressively loaded by a stress wave generated through the collision of the striker and incident bars. Initially, the stress wave, known as the incident pulse, ε_I , travels through the incident bar. Once the incident pulse reaches the sample and transmission bar interface it is partially reflected back through the incident bar, while the remainder travels into the transmission bar. These are referred to as the reflected, ε_r, and transmitted pulses, ε_t, respectively. An illustration of the signal acquired during a SHPB test is shown in Fig 6. The strain rate, $\dot{\varepsilon}$, of the deforming material can be expressed as a function dependent on the velocity of the bars:

$$\dot{\varepsilon}(t) = \frac{(v_1 - v_2)}{L_{sp}} \tag{1}$$

Where v_1 and v_2 are the velocities of the front and back surfaces of the sample, respectively. The velocities of the front and back surfaces of the sample are proportional to the strains generated in the bar and the speed of the propagating wave C_B and are given by:

$$V_1 = C_B(\varepsilon_I - \varepsilon_r) \tag{2}$$

$$V_2 = C_B\varepsilon_t \tag{3}$$

By combining equations (2) and (3) into equation (1), the relationship of the sample deformation speed to the incident, reflected and transmitted pulses can be expressed as follows:

$$\dot{\varepsilon}(t) = \frac{C_B}{L_{sp}}[\varepsilon_I(t) - \varepsilon_r(t) - \varepsilon_t(t)] \tag{4}$$

When the sample reaches dynamic equilibrium the strain at the incident bar interface equals that of the transmission bar interface.

$$\varepsilon_I(t) + \varepsilon_r(t) = \varepsilon_t(t) \tag{5}$$

By using equation (5) the equation describing the strain rate of the sample can be simplified to:

$$\dot{\varepsilon}(t) = \frac{-2C_B}{L_{sp}}[\varepsilon_r(t)] \tag{6}$$

Finally, by using the transmitted strain pulse the stress on the sample can be described by the following equation:

$$\sigma_s(t) = \frac{EA_b}{A_s}[\varepsilon_t(t)] \tag{7}$$

Under the assumption of dynamic equilibrium equations (6) and (7) can be used to directly acquire the stress and strain-rate of the sample as a function of time. The dynamic equilibrium

state of the sample can be evaluated by using equation (7) and replacing $\varepsilon_t(t)$ with $\varepsilon_I(t) + \varepsilon_r(t)$. Equilibrium is assumed in the region where the summation of the incident and reflected pulses oscillated about the transmitted pulse by a difference of roughly 10%, this is illustrated in Fig. 7. The equations stated above only hold true under the assumptions of 1 dimensional wave propagation, frictionless contact, dynamic equilibrium, and no wave dispersion.

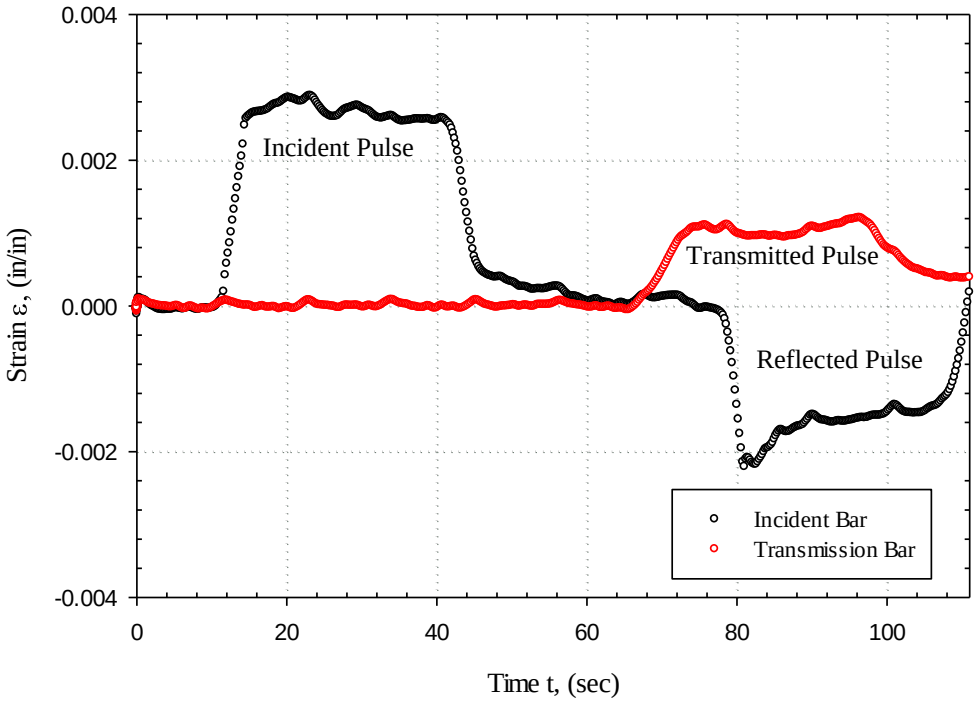

Figure 6. Acquired signal from incident and transmitted bars.

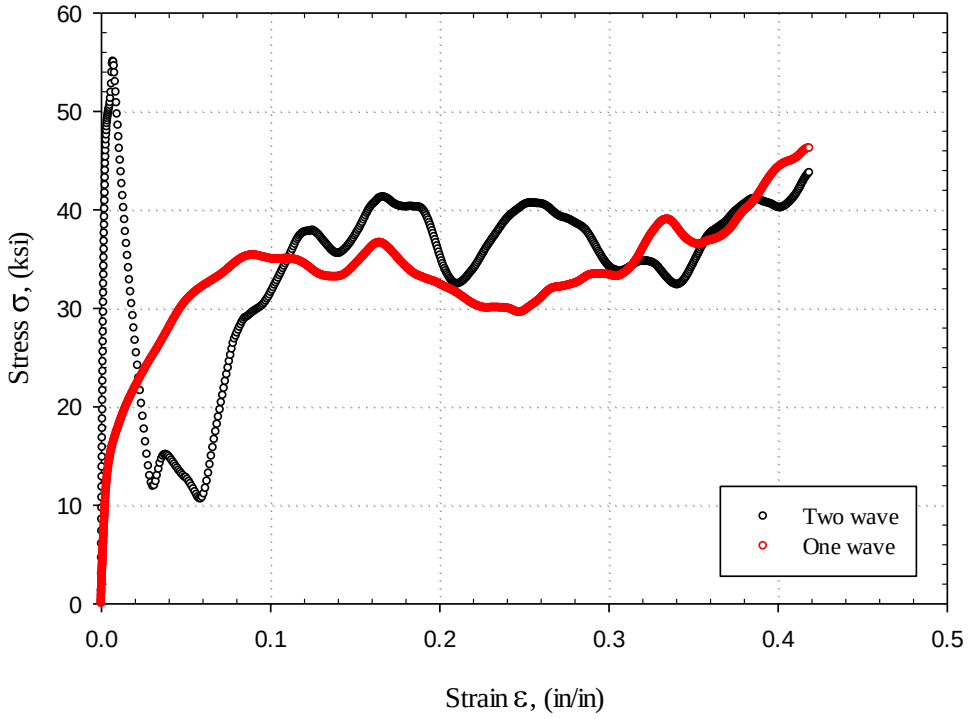

Figure 7. Two wave signal oscillating about the one wave signal.

3. QUASI-STATIC EXPERIMENATION

3.1 Experimental Procedure of Tensile Testing

In order to investigate the tensile properties of the material, several uniaxial tensile experiments were performed on PEI samples at room temperature. To ensure accuracy of the acquired data, all tests were performed in accordance to their ASTM Standard [ASTM D638, 2010]. As-received plate PEI was precision milled into standard Type I rectangular cross section samples. The samples featured an outer radius, R_o , of 0.75 in (19.1 mm), an inner radius R_i , of 0.50 in (12.7 mm), a gage section L_o ,of 2.0 in (50.8 mm), and a thickness, t, of 0.094 in (2.39 mm). To ensure that sample failure occurred within the gage section, a fillet of radius, ρ , of 3.0 in (76.2 mm) was introduced just outside the gage area.

Experiments were performed using a universal test machine (MTS model Insight 5) with a 5 kN load cell operating at a cross head velocity of 0.20 in/min (0.51mm/min). An axial extensometer MTS model 634.11 was used to measure strain to standard and with high precision [ASTM E83a, 2010]. The test coupon and fixture are shown in Fig 8. Fractographic analyses of the test coupons were performed in order to characterize mechanisms of rupture; these images are shown in Fig. 9. To properly acquire the plastic response of PEI beyond the limit of the extensometer, the cross-head displacement was used.

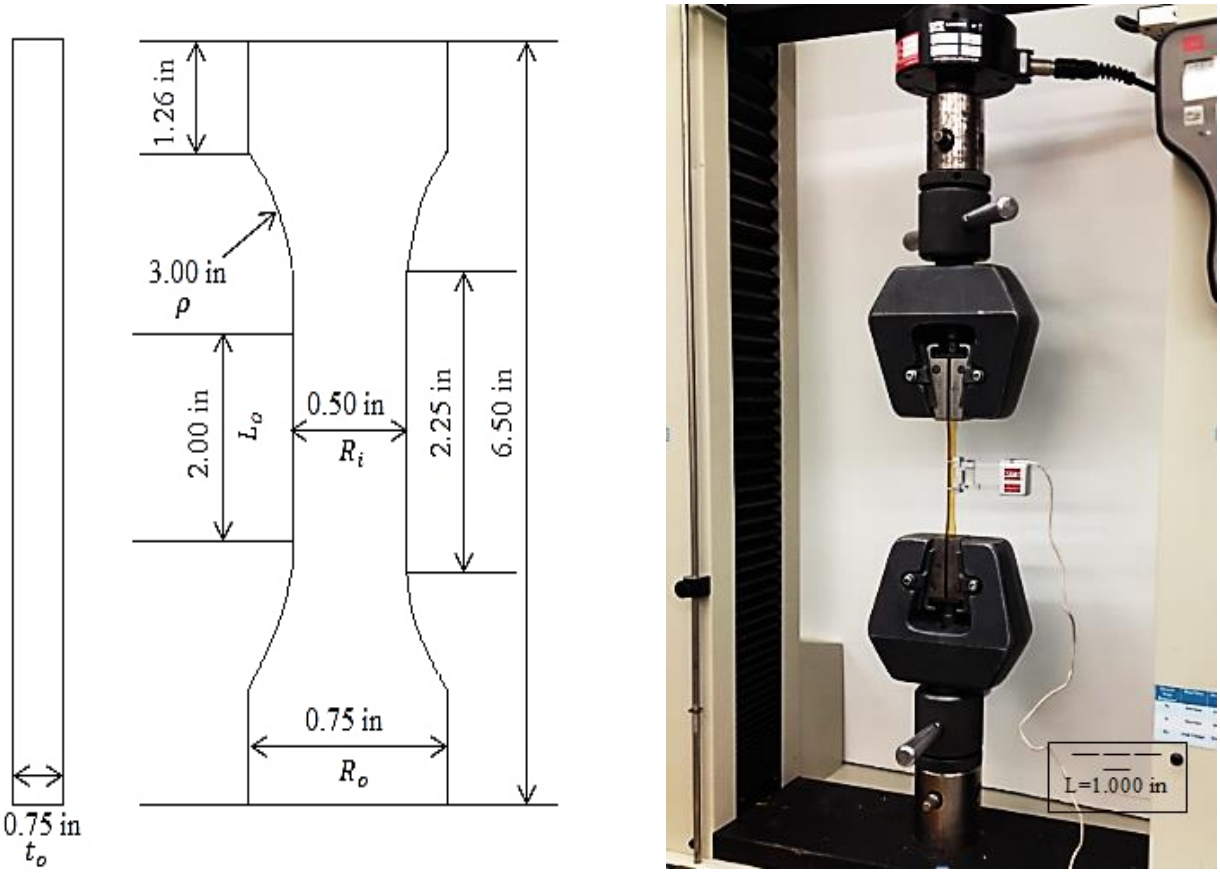

Figure 9. (a) Standard tensile sample with dimensions, and (b) universal test frame

Figure 8. Fracture Surfaces of Standard tensile samples

3.2 Compression Experiments

3.2.1 Experimental Setup and Procedure

Quasi-static compression experiments were designed and perfomed in accordance to the appropriate ASTM Standard [ASTM D695, 2010]. Cylindrical samples were machined from as-received rod material to dimensions of 0.25 in (6.35 mm) by 0.5 in (12.7 mm), and were subjected to compressive load at a crosshead velocity of 0.050 in/min (1.3 mm/min). Experiments were performed on an MTS insight 5 mechanical unit, and the experimental setup is shown in Fig 10. In order to prevent barreling of the samples precautionary actions were performed to lower the surface friction at the sample interface. Surface finishing of the samples and compression plates were performed using 600 grit silicon carbide papers, and lubrication was applied at the interface using a molybdenum disulfide film lubricant (Drislide Multi-Purpose).

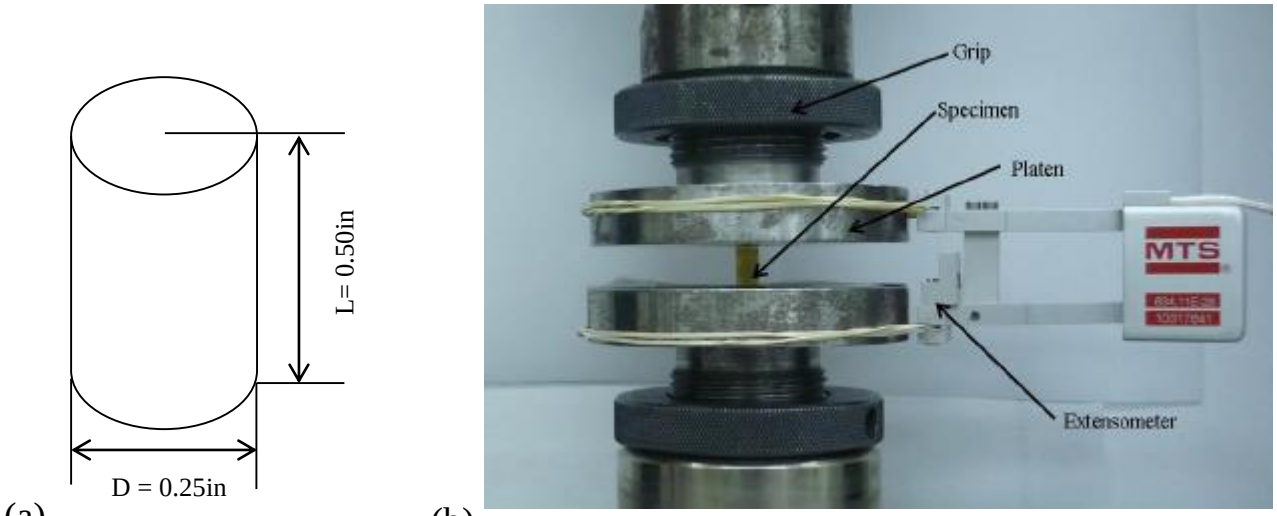

Figure 10. (a) Standard compression test specimen , and (b) universal test frame.

3.2.2 Naturally Aged and Rejuvenated Experiments

In order to study the effects of physical ageing on the mechanical properties of PEI, rejuvenation processes were performed on the material samples and compared to the quasi-static case. Two commonly used processes which work to decrease strain localization in polymers are mechanical and thermal rejuvenation. Mechanical rejuvenation refers to the deformation of the polymer well beyond its yield strength, which lowers the yield strength of the material. Thermal rejuvenation refers to the process of heating a polymer above the glass transition temperature, and then quenching the material causing the polymer chains to return to a high energy state. In this experiment, mechanical rejuvenation was accomplished by pre-deforming Ultem 1000 specimens to 12% strain, while thermal rejuvenation was achieved by heating rod material to 235 °C for 30 min, then quenching the material in water to room temperature.

3.3 Experimental Setup and Procedure for Torsion Experiments

Quasi-static torsion experiments were performed on as-received PEI samples at room temperature. In illustration of the torsion sample in fixture is provided in Fig. 11. Samples were machined from rod material to solid cylinders with dimensions corresponding to specifications of the appropriate ASTM standard [ASTM E143, 2010]. The gage length and diameter of the samples measured 2.25 in (0.057 m) and 0.235 in (0.006 m), respectively. Experiments were performed on an MTS (Bionix 45 N-m) testing frame, and at a speed of 5 revolutions per minute corresponding to strain rates on the order of 10^{-2}/s.

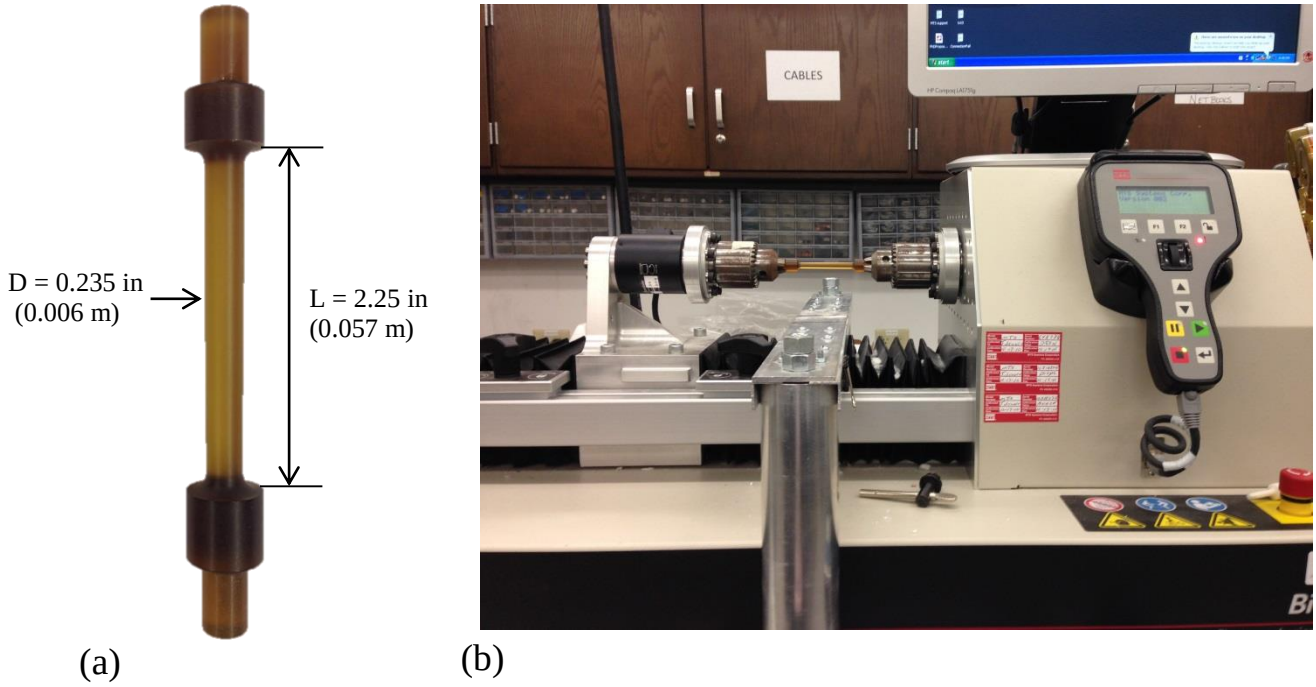

Figure 11. (a) Standard Torsion Specimen, and (b) testing fixture.

4. HIGH STRAIN RATE EXPERIMENTS

4.1 Charpy Impact Experiments

To study the mechanisms of failure as a response to high strain rate deformation, Charpy Impact experiments were performed at room temperature using a universal impact test machine (Instron Model SI-1B) on as received Poly(etherimide). Plate material was machined into Type A notched impact samples in accordance to the appropriate ASTM standard [ASTM E23, 2012]. The PEI sample and Charpy Impact test fixture is shown in Fig. 12. The samples had a total length, L, of 2.165 in (55 mm), a height, H, of 0.394 in (10 mm) and thickness ,T, of 0.394 in (10 mm), a notch depth, D, of 0.039in (1.0 mm), with an angle ,P, of 45°, and radius of the notch, *R*, of 0.001 in (0.25 mm). To evaluate the properties of Poly(etherimide) the pendulum of the impact test machine was set at a height, H_p, of 1.88 ft (0.573 m), resulting at an impact velocity, V_p, of 11.0 ft/s (3.35 m/s) corresponding to strain rates on the order of 10^2/s. This height corresponds to the lowest possible starting height of the pendulum.

To quantitatively analyze the mechanisms of failure, fracture surface photographs were captured and the fracture appearance of the samples were compared to percent shear fracture comparators provided in the ASTM standard. The common post impact fracture surfaces are shown in Fig. 13. Finally, the area of the sample was measured post examination to determine the percent of lateral expansion.

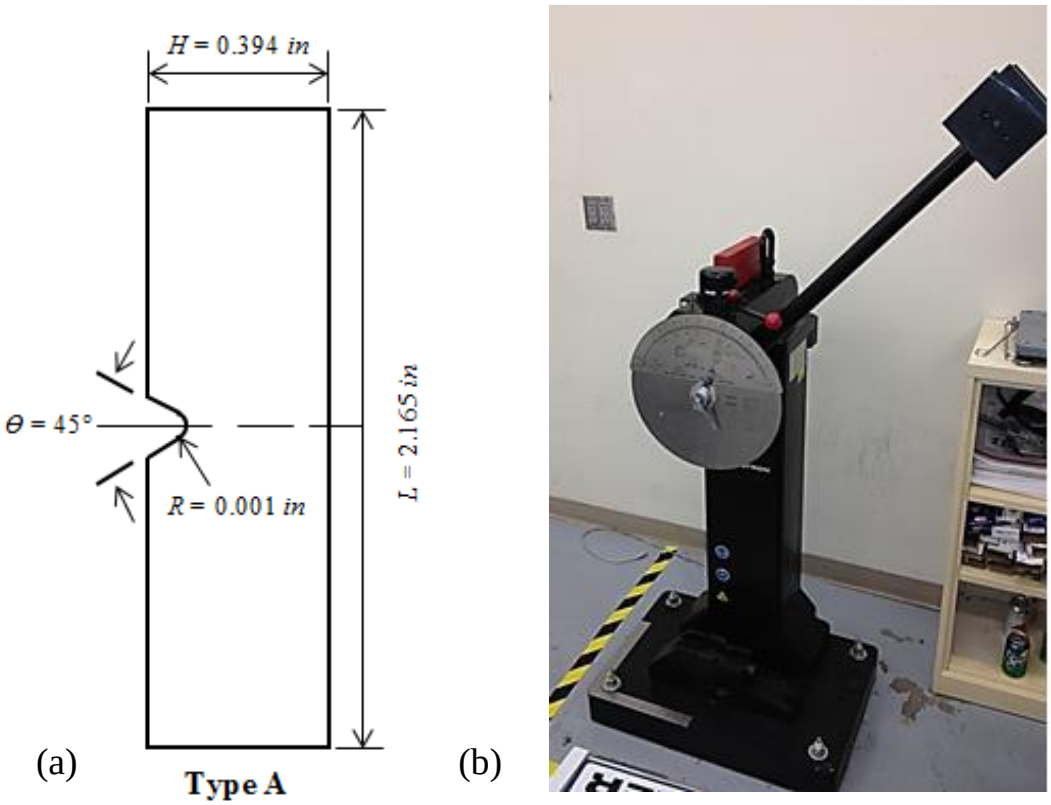

Figure 13. (a) Standard Type A Impact sample, and (b) Charpy Impact test fixture.

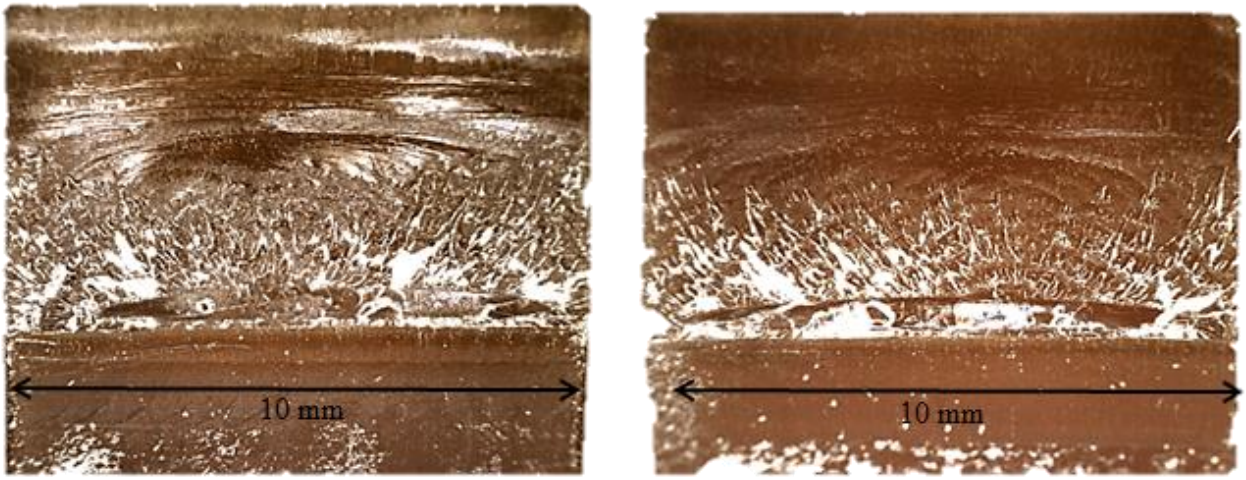

Figure 12. Fracture surfaces of standard Charpy Impact samples.

4.2 Split Hopkinson Bar Experiments

4.2.1 Experimental Setup and Procedure

For this experiment, PEI was machined to a right circular cylinder using a miniature lathe, and then sanded using a custom jig to a diameter, D_s, of 0.070 in (1.83 mm) and a length, L_{sp}, of 0.039 in (1.00 mm). An illustration of the mSHPB samples is provided in Fig 14. Specimens with a length to diameter ratio of nearly 0.50 were carefully chosen in order to prevent barreling of the samples, radial inertial effects, and interfacial friction between the specimen and bars [Davies, 1948; Gray, 1977; Chen, 2011]. The experiments were conducted using a miniaturized Split Hopkinson Pressure Bar (MSHPB) at high strain rates of 10^4/s. The mSHPB is fundamentally identical to the SHPB apart from the reduction in size. Shown in Fig. 15 is the experimental setup. The mSHPB consists of incident and transmitted Aluminum 7075-T6 bars each of 10.0 in (254 mm) length and 0.125 in (3.175 mm) diameter, and a striker bar of the same diameter and length 3.00 in (76.2 mm). Further details about the setup and data acquisition system can be found in the Thesis by Nathan Mutter [Mutter, 2011]. The next section will discuss the calibration methods used for this experiment.

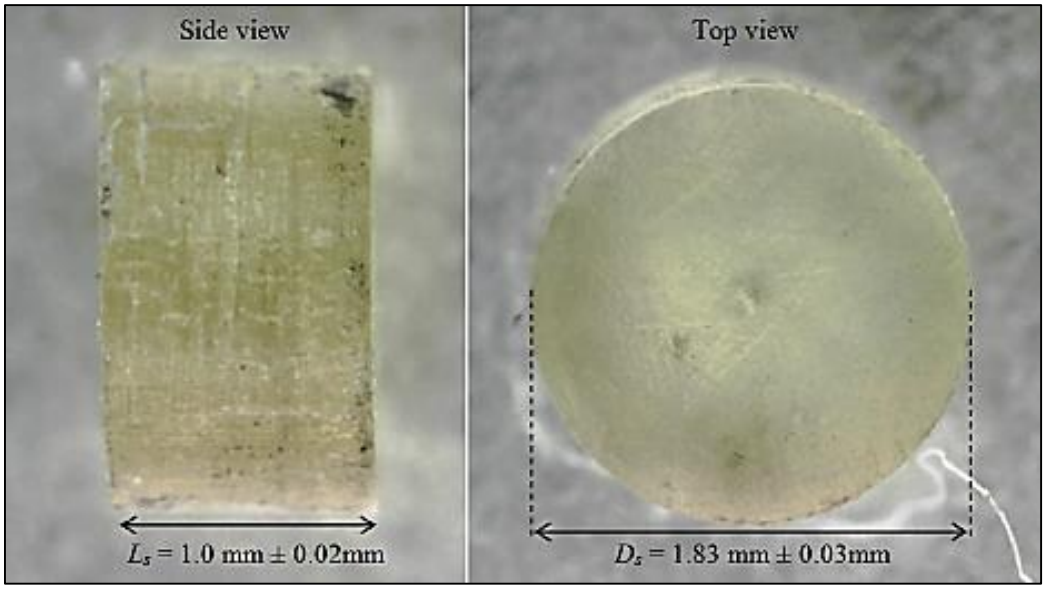

Figure 15. Side view and top view of a sample used for mSHPB experimentation.

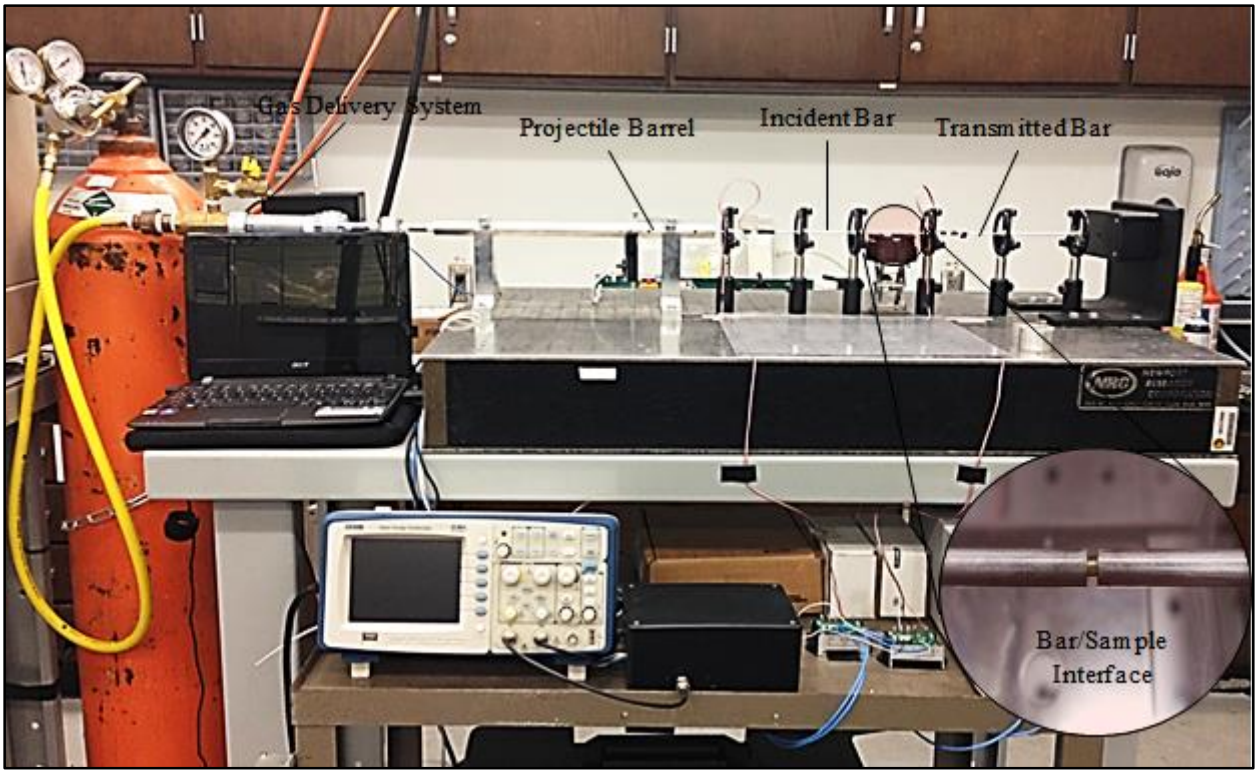

Figure 14. Minituare Split Hopkinson Pressure Bar loaded with PEI samples.

4.2.2 Calibration

In experimental techniques such as the SHPB it is vital to maintain an accurate calibration to ensure the precision of acquired data. Prior to this investigation the newly built mSHPB was subjected to a comprehensive calibration procedure. First, the gas gun chamber was subjected to varying pressures in order to determine fire speed and repeatability. The pressure of 50 psi was determined to project the striker bar at a speed of 15m/s by means of a photo gate. Second, the gain of the amplification system was determined by plotting the input versus output voltages, the result is shown in Fig 16.

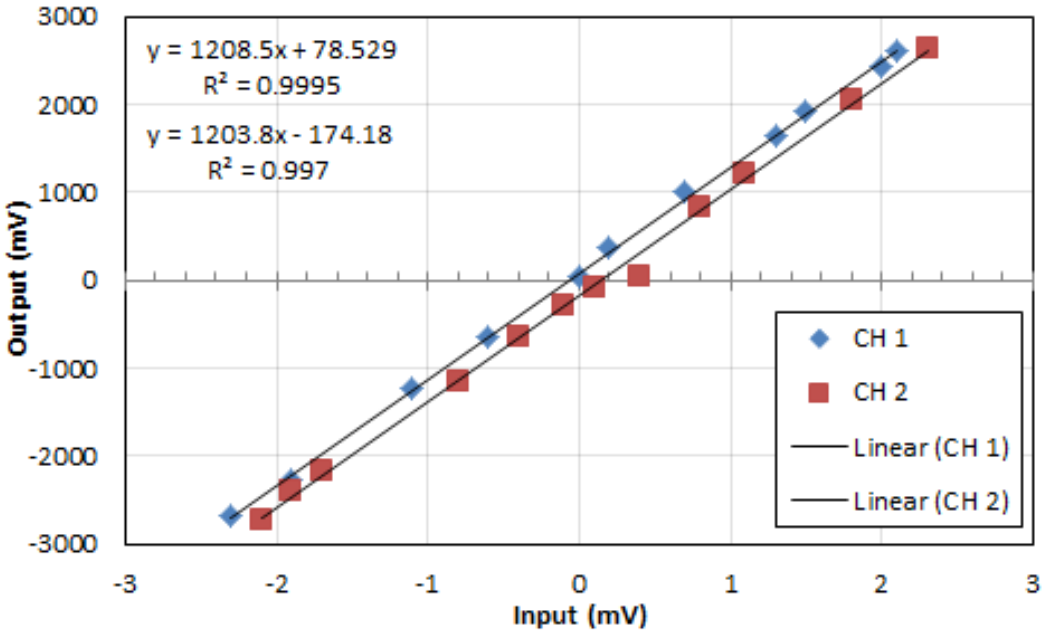

Figure 16. Ch1 and Ch2 gain calibration for amplification system.

Next, the signal acquired from the strain gages was calibrated. Using the following relationship

$$\sigma_B = \frac{1}{2}\rho_B C_B V_{st} \tag{8}$$

where, ρ_b, and $C_{b,}$ are the density and wave speed of the bar, respectively, the theoretical stress generated by the bar was determined based on the striker velocity. By dividing the theoretical stress from equation (8) by the Young's modulus of the bar the theoretical strain of 0.2175 (in/in) was determined. By performing "bars together" experiments the magnitude and transmission of the experimental strain pulses were acquired. By comparing the magnitude of the experimental strain pulses to the theoretical strain pulse, the calibration constants of 1.084 and 1.061 were determined for the incident and transmission bars, respectively. The calibrated signal is plotted versus the theoretical maximum shown in Fig. 17.

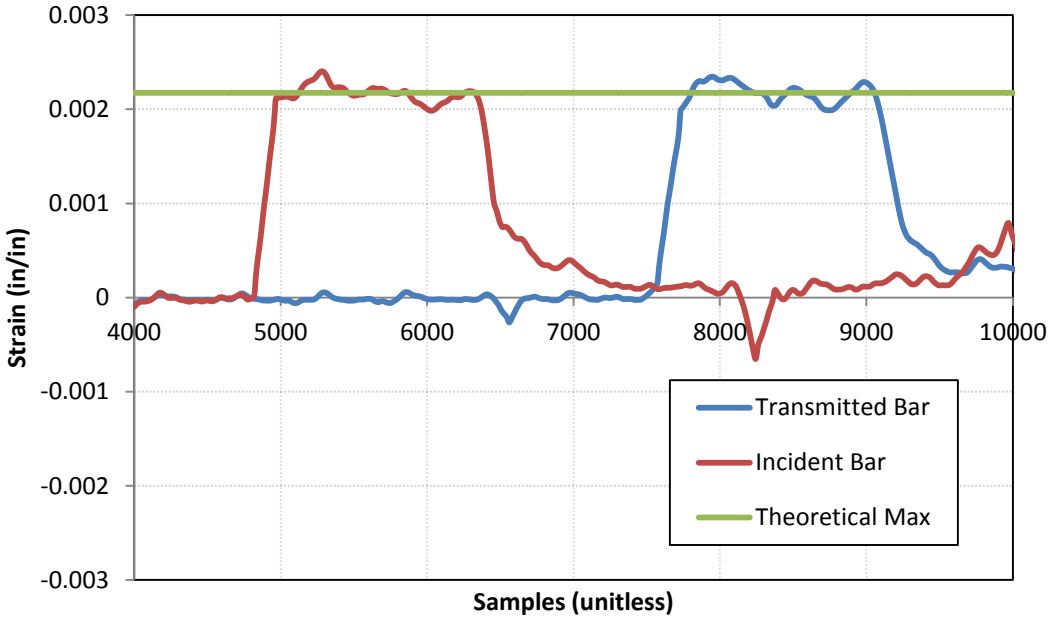

Figure 17. Calibrated strain pulses acquired from incident and transmission bars.

From the figure it is shown that the calibrated incident bar signal adequately reaches the theoretical strain and propagates from the incident to the transmitted bar.

In order to maintain the assumption of one dimensional wave propagation it was necessary to ensure that the mSHPB sample was aligned to the center of the bar interface. To precisely align the sample a custom alignment jig was developed our of stainless steel and PLA and is shown in Fig. 18.

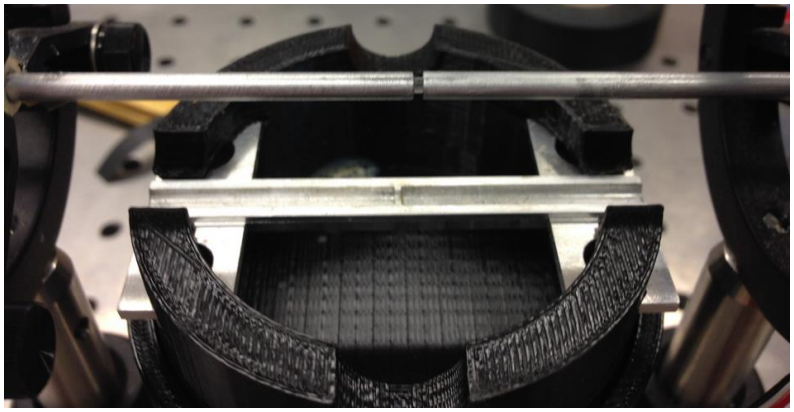

Figure 18. Custom sample alignment fixture for mSHPB.

Furthermore, an enclosure was developed in order to capture the sample during post testing, and this enclosure is shown in Fig. 19.

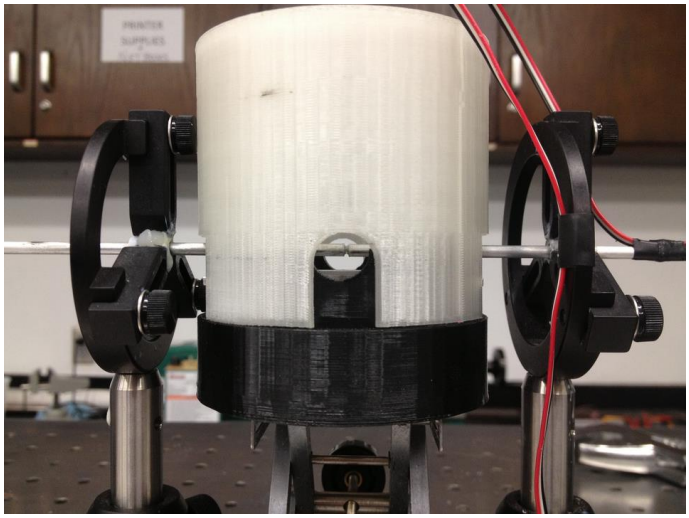

Figure 19. mSHPB sample capture enclosure.

5. EXPERIMENTAL RESULTS

5.1 Quasi-Static Tension

It has been noted that the mechanical responses of several polymers are marked by four distinctive mechanical regimes before rupturing: (1) linear elastic, (2) non-linear elastic, (3) strain softening, and (4) strain hardening [Brown, 1968]. Similarly is the response of PEI. Shown in Fig. 20. The linear elastic regime is a result of van der waal forces present during interactions between polymer chains as they slide with respect to one another. The linear elastic regime is used to calculate the Young's modulus of the material, averaged at 470 ksi (3.24 GPa). As deformation continues, localization within the sample increase the level of stress until it finally overcomes the van der waal forces and causes the linear response to become notably non-linear, this occurs after the proportional limit (PL) found to be at 1% engineering strain. At roughly 7.3% engineering strain, the material exhibits a local maximum in stress considered the yield strength, and this value was averaged at 15.6 ksi (108 MPa). Upon plastic deformation the tensile curve exhibited a strain softening regime related to volume relaxation attributed to the physical aging process [Struik, 1978, Simon, 1996, Mahajan, 2010]. This mechanical response is a result of reduction in mobility and increase in free volume caused by the polymer slowly shifting towards equilibrium. The consequence of this process is strain localization which leads to a reduced level of stress required for continued deformation. The material then begins to strain harden due to the alignment of the polymer chains in the direction of the force and the reduction of cavity density which requires an increased level of stress for continued deformation [Marano, 2013]. Finally, the sample ruptures after reaching approximately 80% engineering strain, at a stress of 13.6 ksi (89.6 MPa).

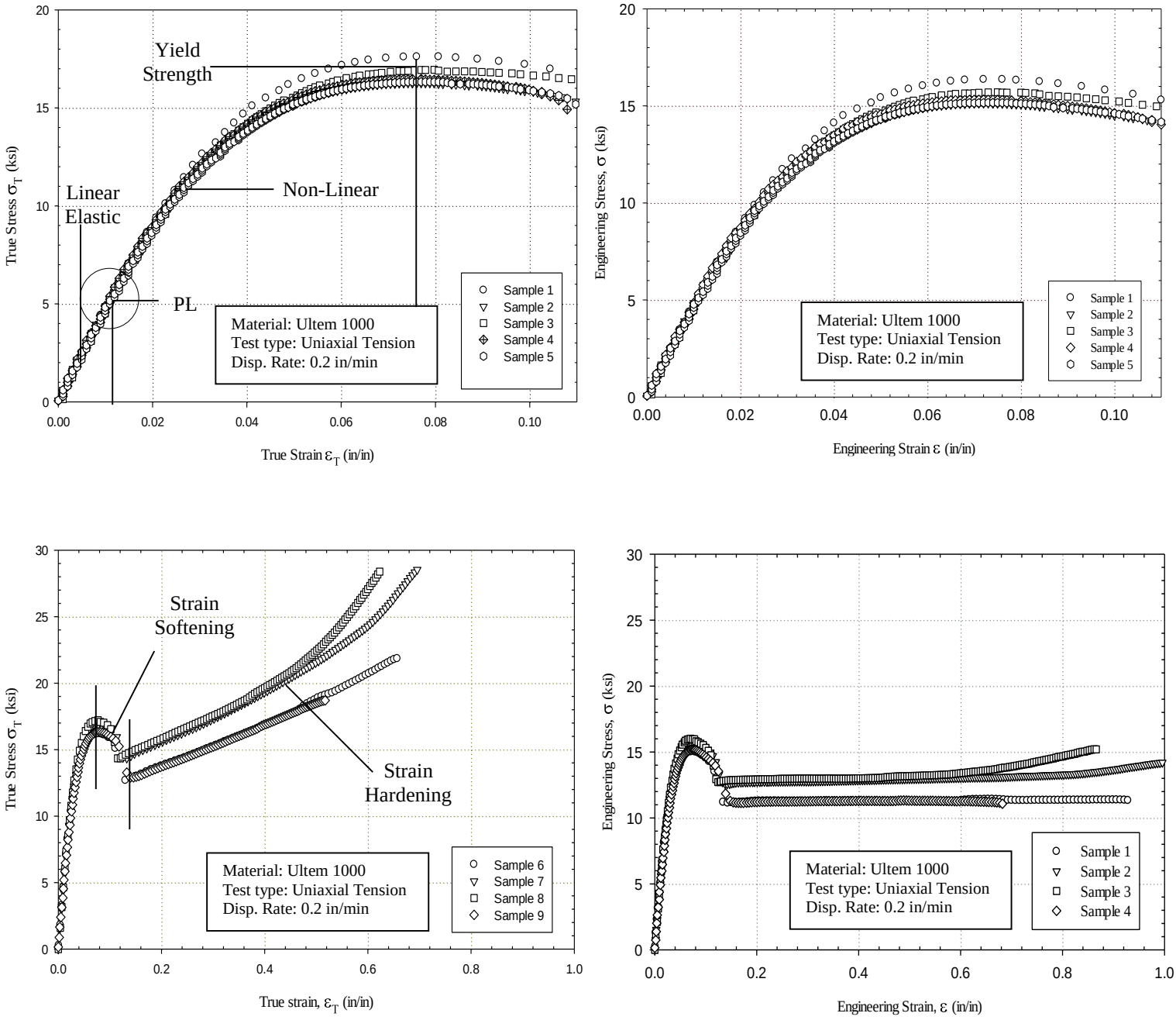

Figure 20. Mechanical response of PEI to uniaxial Tension.

An analysis of the fractured tensile samples was performed in order to characterize the mechanisms of rupture. The fracture surfaces of several tensile samples are shown in Fig. 21. During deformation a stress concentration was the origination point for a slow growing crack characterized by a nominally flat and uniform region in the vicinity of the defect. Once the crack reached critical proportions a sparse region characterized the transition between a slow growing crack and a fast fracture. The stress levels generated by the test exceeded the load bearing capacity of the sample causing a fast fracture, and the presence of shear lips and dimples indicated a ductile overload. The fracture surface features mentioned above are consistent among the tensile samples.

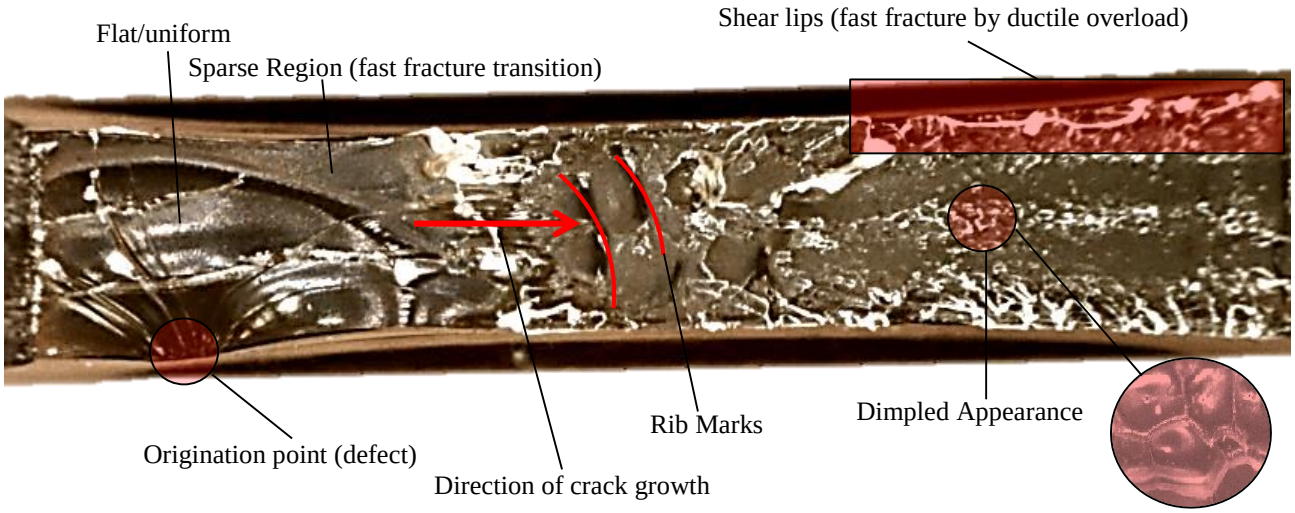

Figure 21. Macro-scale fracture surface of the Ultem 1000 samples after uniaxial tension.

5.2 Quasi-Static Compression

5.2.1 As-received PEI Testing

Similar to the quasi-static tensile behavior of as received Ultem 1000, the compressive mechanical response is marked by four mechanical regimes. (1) linear elastic, (2) non-linear elastic, (3) strain softening, and (4) strain hardening. The compressive strength curve for Ultem 1000 is provided in Fig 22. The linear elastic regime is caused by the resistance to deformation due to the van der Waal forces which attract the polymer chains to one another. This regime lasts until about 1% engineering strain, and is used to calculate the compressive Young's Modulus, E_c, which averages 480 ksi (3.31 GPa). Subsequent to the linear elastic behavior is the non-linear elastic regime, caused by the polymer chains sliding with respect to one another. At roughly 8.7% engineering strain the material yields at 22 ksi (152 MPa). Upon yielding the specimen strain softens, and then continues to strain while hardening until finally buckling at about 30 ksi (207 MPa) and 40% engineering strain.

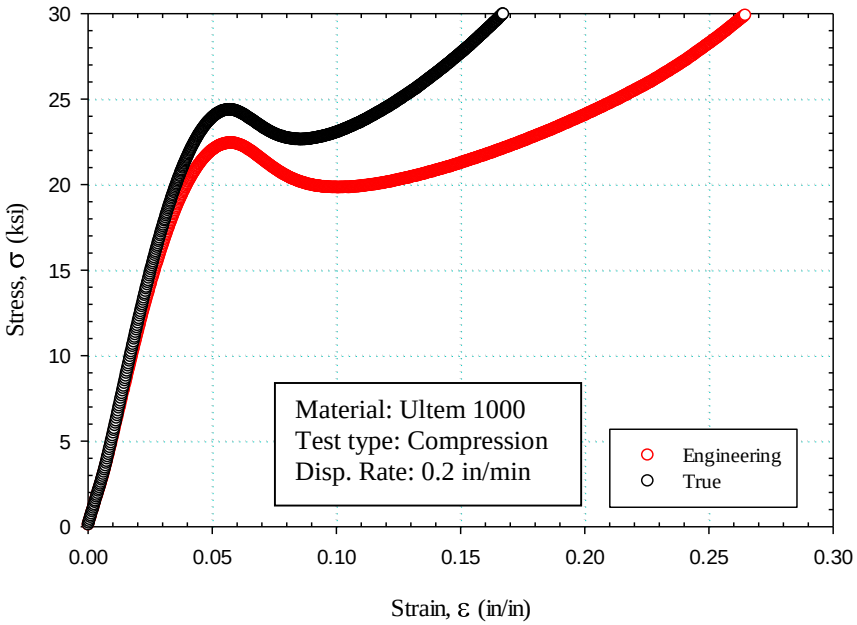

Figure 22. The mechanical response of Ultem 1000 to uniaxial compressive loading.

5.2.2 Rejuvenation Experiments

The mechanical response of Poly(etherimide) to uniaxial compression post rejuvenation is shown in Fig. 23 and Fig. 24. The mechanical and thermal rejuvenation processes were shown to be nearly identical in lowering the yield stress of the material 20% from 22ksi (152 MPa) to roughly 18 ksi (124 MPa), and both processes completely eliminated the strain softening regime and thus hindered strain localization. Thermal rejuvenation should be induced under a vacuum to prevent the formation of cavities, and dimensional changes within the sample. A decrease in ductility amounting to nearly 4% was induced by mechanical rejuvenation; however, this impact in the ductility was not evident in the experiments considering that the samples buckled before reaching their maximum elongation. Mechanical and thermal rejuvenation were shown to be exceptional methods of reducing the strain softening regime in the response of the material.

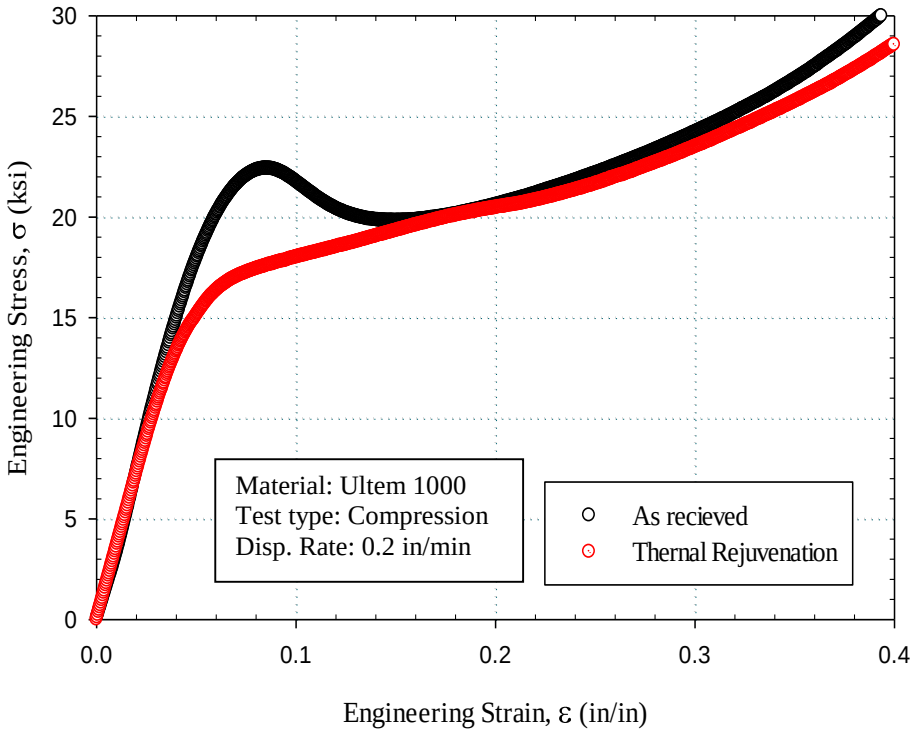

Figure 24. Mechanical Response of PEI to compression post thermal rejuvenation.

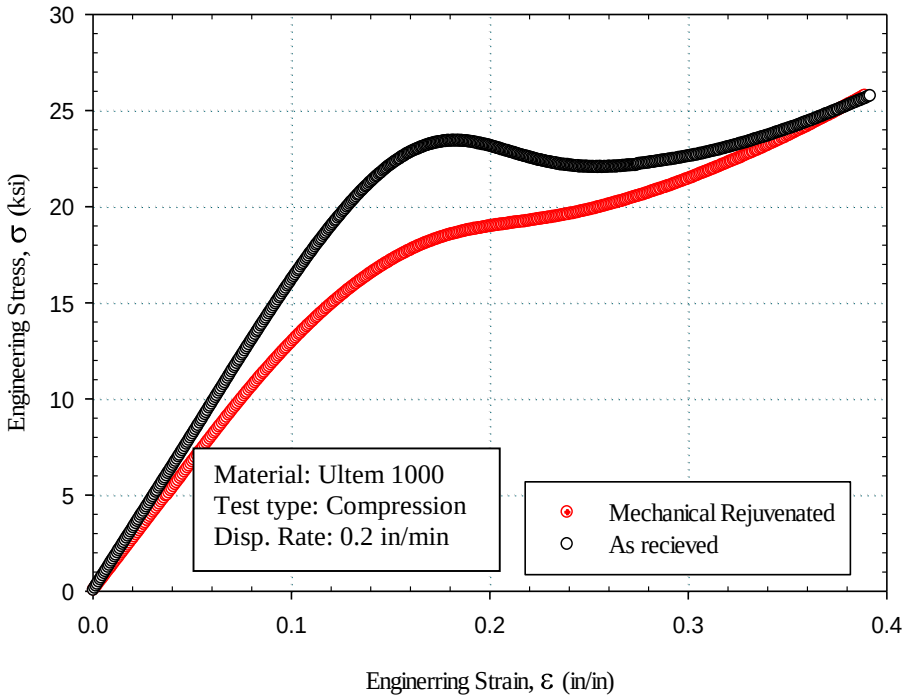

Figure 23. Mechanical response of PEI to compression post mechanical rejuvenation.

5.3 Quasi-Static Torsion

Similar to the quasi-static deformation of as-received PEI, the material initially responds to shear stress linearly. The elastic response of as-received PEI is compiled in Table 5, and illustrated in Fig 8. The shear modulus, G, is the slope of the linear regime and is measured to be 174.4 ksi (1.2 GPa), and expressed as

$$G = \frac{E}{2(1+\nu)} \tag{9}$$

that compares the shear and Young's modulus, the Poisson's ratio, ν, is found to be 0.362. The linear regime ceases at the proportional limit, PL, occurring at just over 1% engineering strain. The response following the linear elastic regime is shown to be non-linear. At nearly 15% engineering strain the material exhibits a local maximum in strength; this value is regarded as the yield strength and is measured at 14.0 ksi (96.3 MPa).

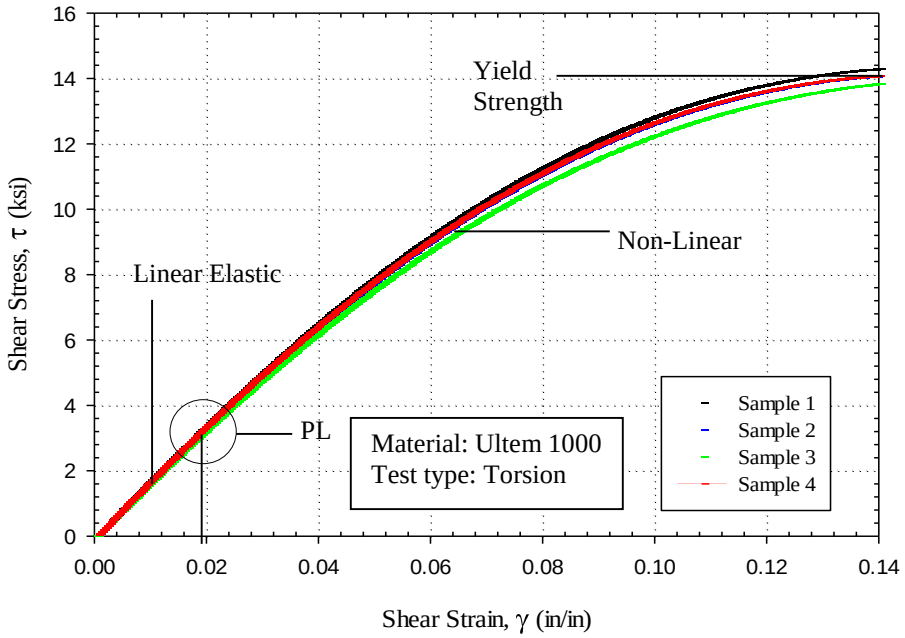

Figure 25. The mechanical response of PEI to uniaxial torsion.

5.4 Charpy Impact Testing

With the pendulum of a mass,M_p, of 13.3 lbs (6.03 kg) the anvil supplied a total impact energy, E_p, of (25.0 ft-lbs) 33.9 *J*. At this energy, the Poly(etherimide) samples did not absorb any measurable energy. To analyze the failure mechanisms of the samples, macro-scale fracture surface images are shown in Fig. 26. It can be observed that the samples did not display any lateral expansion, nor did they possess shear lips/area. From the analysis, it can be deduced that in the presence of a notch and at the specified impact energy, Poly(etherimide) will consistently respond to impact by brittle fracture.

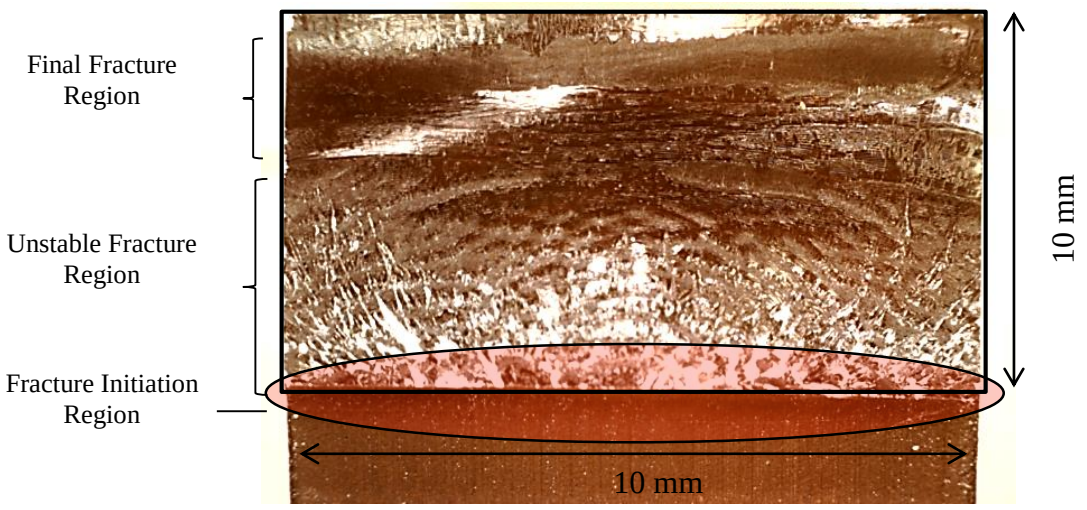

Figure 26. Macro-scale fracture surfaces of Ultem 1000 samples post Impact.

5.5 Split Hopkinson Pressure Bar

Using the Split-Hopkinson Pressure Bar technique Ultem 1000 specimens were compressively deformed to nearly 50% engineering strain, at roughly 15,000/s strain rates. The equilibrium regions were determined by comparing the one wave and two wave curves, this is shown in Fig. 27. The stress acquired during the test is shown in Fig 28a and the stress-strain response of this material is shown in Fig. 28b. By using Eq. (5) in conjunction with Eq. (7) the specimens were determined to reach a point of dynamic equilibrium in a range of 2-4% engineering strain, hence, a linear regression between this point and the point of zero deformation was used to determine a stiffness estimate of the material of 447 ksi (3.08 GPa). This approximation was compared to E of the statically deformed compression samples which showed that the elastic response of the sample did not change significantly as a function of strain rate, as shown in Fig. 28c; however, the strength of the material clearly shows strain-rate sensitivity. The material exhibits a bilinear behavior in its sensitivity to strain rate, and displays a transition region at around 10^3/s similar to that of poly(propylene) and poly(vinyl chloride) [Walley, 1991], this result is illustrated in Fig 28d. The upper yield strength of the material was averaged at 36.1 ksi (248 MPa), and the lower yield strength of the material at 31.0 ksi (213 MPa). This result is significantly larger than that of the statically deformed samples averaged at 22.4 ksi (154 MPa) and 12.0 ksi (82.7 MPa).

Considering the bilinear trend of the strength sensitivity of PEI to strain-rate, this behavior was correlated using the Ree-Erying equation. The equation takes the form:

$$\frac{\sigma_y}{\theta} = A_1\left[\ln(2C_1\dot{\varepsilon}) + \frac{Q_1}{R\theta}\right] + A_2 \sinh^{-1}\left(C_2\dot{\varepsilon}e^{\frac{Q_2}{R\theta}}\right) \tag{10}$$

Here, A_i is a material parameter with units *Pa/°K*, C_i is a material parameter with units seconds, Q_i are the activation energies associated with each process *kcal/mol*, R is the universal gas constant, and θ is the absolute temperature of the material [Ree, 1955]. The parameters of the model were determined from fitting experimental data and are shown in Fig. 28d. The results show that the deformation response of this material at higher strain rates follows a similar shape as that of the statically deformed specimen, but at an amplified stress. The strength of the material at 15,000/s strain rate was shown to be up to 170 % that of the quasi-static case.

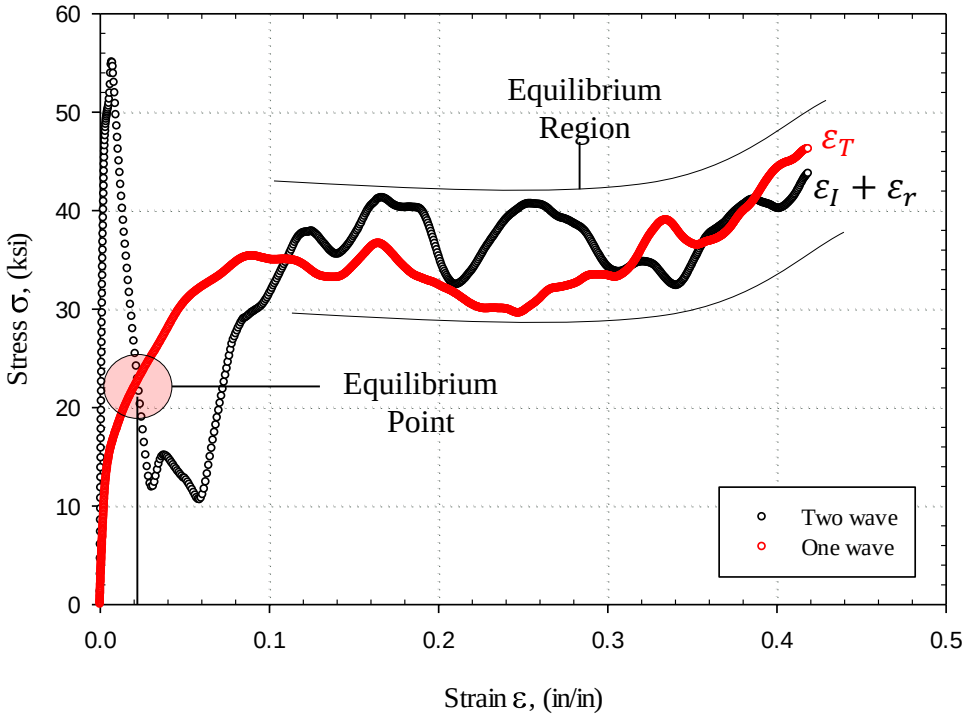

Figure 27. One wave and two wave stress signals, and dynamic equilibrium region.

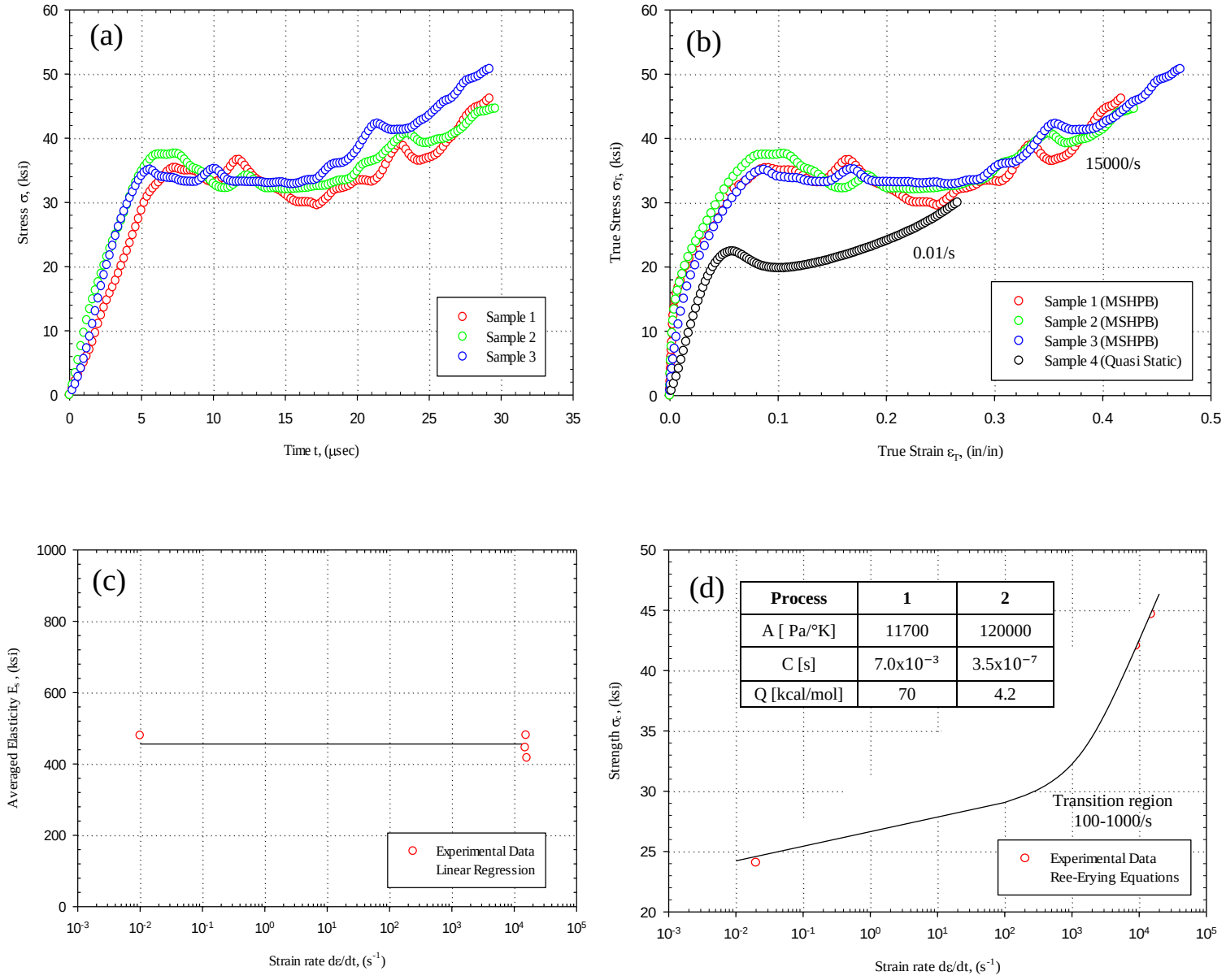

Process	1	2
A [Pa/°K]	11700	120000
C [s]	$7.0x10^{-3}$	$3.5x10^{-7}$
Q [kcal/mol]	70	4.2

Figure 28. Comparison between high-strain rate and quasi-static response of Polyethermide to uniaxial compressive loading.

6. Modeling

6.1 Monotonic Modeling

In order to determine the mechanical response of the Poly(etherimide) to quasi-static loading, a model was implemented by using the Ramberg-Osgood strain equation in conjunction with a novel model. The implementation of this model is practical for correlating the behavior of the material, as well as, finding uncertainties within a set of data. The Ramberg-Osgood strain equation was used to model the elastic regime of the material due to the ease in determining the parameters to fit the curve. The equation takes the form

$$\varepsilon = \frac{\sigma}{E} + \alpha\left(\frac{\sigma_o}{E}\right)\left(\frac{\sigma}{\sigma_o}\right)^n \tag{11}$$

where σ_o is the 0.02% offset yield stress, respectively; both α and n are parameters that describe the yield point and hardening behavior of the material. By evaluating the equation at the yield strain ε_o, α is expressed as:

$$\alpha = \left(\frac{E\varepsilon_o}{\sigma_o}\right) - 1 \tag{12}$$

The equation can be further evaluated at an arbitrary stress σ_1 and re-arranged to solve for the parameter n. The equation is as follows:

$$n = \frac{\ln\left[\frac{E}{\sigma_o \alpha}\left(\varepsilon_1 - \frac{\sigma_1}{E}\right)\right]}{\ln\left(\frac{\sigma_1}{\sigma_o}\right)} \tag{13}$$

By using the parameters α and n (0.053 and 11.92, respectively), the Ramberg-Osgood model was used to fit the elastic regime of the rejuvenated material response to compression, as shown in Fig 29a. This model was also used to correlate the elastic response of as-received PEI, to quasi-static tension, torsion, and compression. The material and hardening constants for these quasi-static cases can be found in Tables 3-5, the result is illustrated in Fig 29b. The Ramberg-Osgood model provided an excellent fit for the data and validated the model's ability to capture the elastic response of PEI.

Although the Ramberg-Osgood model correlated well with the material deformation up to 12% engineering strain, it did not accurately capture the strain hardening response. In order to capture hardening of the material at higher strains a more sophisticated model was required. Hooke's Law was used to model the initial linear response of the material, and an inverse exponential equation was added in order to model the non-linear elastic and plastic behavior of the material. The equation becomes

$$\varepsilon = \frac{\sigma}{E} + C_1\left[C_2 + \exp\left(\frac{\sigma_{ref}}{\sigma}\right)\right]^{-1} \tag{14}$$

where C_1, C_2, and σ_{ref} are model parameters. The model parameters were determined by regression fit. The parametersC_1 and C_2 were found to be 703 and 1860, respectively, while σ_{ref}

was found to be 23.1 ksi (159 MPa), respectively. The result of this model can be seen in Fig 29c. Equation (13) correlates well with the elastic and plastic behavior of the material. The maximum error of the model valued at 4.5% occurs at the 0.02% yield strength.

In order to fully capture the elastic and plastic behavior of the material a piece-wise equation was implemented by combining equations (13) and (10). The Ramberg-Osgood equation was used to model the material response until 12% engineering strain, and an inverse exponential relationship was used to model the material response beyond that point. The piece-wise equation can be expressed as follows:

$$\varepsilon = \begin{cases} \dfrac{\sigma}{E} + \alpha\left(\dfrac{\sigma_o}{E}\right)\left(\dfrac{\sigma}{\sigma_o}\right)^n & 0 \le \varepsilon \le 0.12 \\ \dfrac{\sigma}{E} + C_1\left[C_2 + \exp\left(\dfrac{\sigma_{ref}}{\sigma}\right)\right]^{-1} & 0.12 < \varepsilon \le 0.40 \end{cases} \tag{15}$$

By combining the Ramberg-Osgood equation and the inverse exponential equation, the elastic and plastic response of poly(etherimide) in static conditions is accurately captured for deformations up to 40% strain. This model bears resemblance to the E. Voce one-dimensional plastic hardening model, a practical model with 3 parameters where plastic strain is inversely related to the stress on the material [Voce, 1948, Voce 1955]. The elastic response of as-received PEI was correlated solely using the Ramberg-Osgood equation and is provided in Fig 29d. Future modifications to Eq. (15) will be investigated in order to correlate elastoplastic response of rejuvenated and as-received PEI to multiple rate conditions.

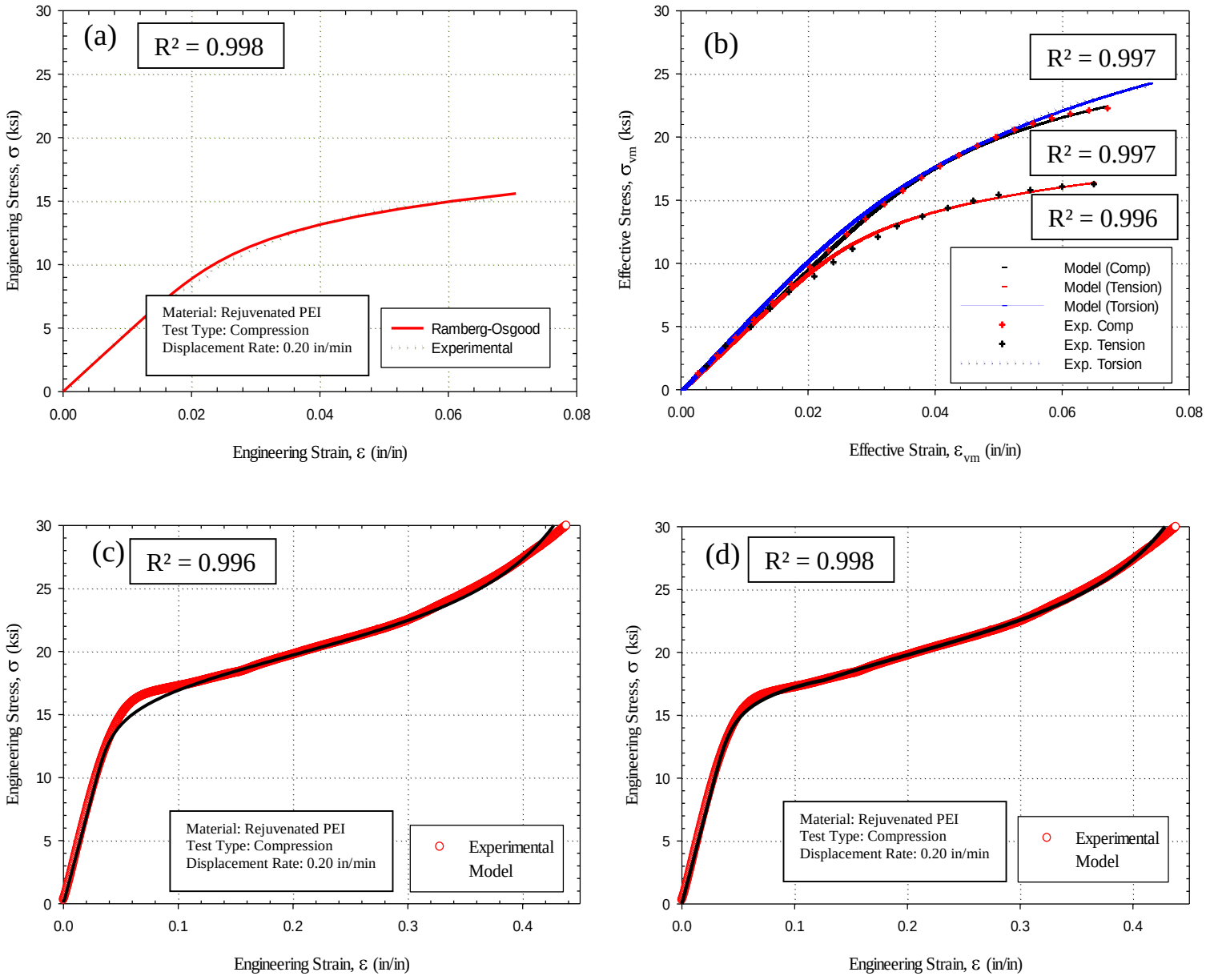

Figure 29. (a) The elastic response of rejuvenated PEI fit with the Ramberg-Osgood equation, (b) the elastoplastic response of rejuvenated PEI fit with the inverse exponential equation, and (c) the elastoplastic response of rejuvenated PEI correlated with the combined equations. (d) The correlated elastic regime of as-received PEI to quasi-static compression, tension, and torsion fit with the Ramberg-Osgood equation.

7. Discussion and Conclusion

The mechanical response of PEI is evaluated at a range of strain-rates and loading conditions. The response of PEI to quasi-static uniaxial tension and compression is found to be consistent to that of other amorphous polymers tested in similar conditions. PEI responds to this loading type by deforming in four distinct mechanical regimes; linear elastic, non-linear elastic, strain softening, and strain hardening. The as-received PEI material exhibits an upper yield strength characterized by a local maximum in the strength curve, this attribute is a result of physical ageing which promotes strain localization within the material, and as a consequence leads to strain softening. The strain softening regime was shown to be avoidable by inducing either mechanical or thermal rejuvenation. Both processes successfully eliminated the strain softening response of PEI, and lowered the yield strength of the material nearly 20%. The mechanical response of rejuvenated PEI was investigated and correlated using a combination of the Ramberg-Osgood model and an inverse exponential equation. This model accurately predicted the response of PEI for deformations up to 40%. The elastic response of PEI to quasi-static torsion was investigated and found to follow a similar trend to that of the tension, and compression case. The shear modulus was measured and compared to the Young's modulus in order to evaluate the Poisson's ratio, which was found to be 0.36. The elastic response of PEI was successfully modeled using the Ramberg-Osgood equation. Next, the failure mechanism of PEI was evaluated under dynamic conditions using a Charpy Impact Test machine, and the material failed predictably and in a brittle manner under the presence of a notch at impact energies of 33.9 J. Finally, the response of PEI to uniaxial compression is evaluated at over 10^4/s strain-rate using a MSHPB. The stiffness of PEI is found to be independent of strain-rate,

however, the strength of the material is found to be strain-rate sensitive. The strength of PEI is found to increase by 70% during the high strain-rate experiments as opposed to the quasi-static case. The strain-rate sensitivity of PEI is found to be bilinear, and was successfully correlated using the Ree-Erying equation.

8. FUTURE WORK

Much future work is still necessary in order to fully characterize PEI. New developments must be made both experimentally and numerically. Experimentally, the rate dependency and mechanical response of rejuvenated PEI will be characterized at a range of high strain rates. Next, the temperature dependency and multi-axial pressure sensitivity of the mechanical response will be investigated. Multiple impact experiments will be performed on as-received and rejuvenated PEI, and microstructural changes in response to impact will be investigated. In order accurately, perform these experiments several modifications will be made to the mSHPB testing apparatus. Low impedance pulse shapers must be developed to allow for constant strain rate experimentation, and optical strain measurement techniques, as well as, high speed CCDs will be used in order to precisely measure strain and evaluate the dynamic equilibrium of the sample. Confinement and strain limitation jigs will be machined in order to run multiple impact experiments at constant strain energies and to apply multi-axial load to the samples. Numerical models have been developed to correlate the elastoplastic response of rejuvenated PEI, however, models that correlate the response of as-received PEI will be developed. Work is be done to modify quasi-static numerical models in order to correlate the response of PEI to a range of deformation rates, preliminary results are shown in Fig. 30.

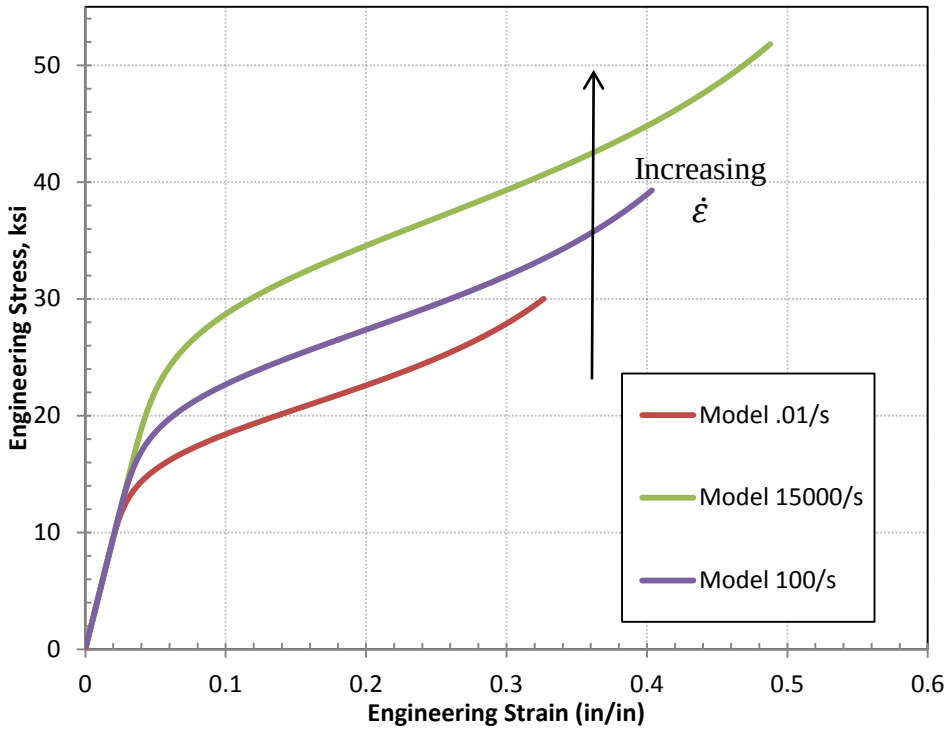

Figure 30. Preliminary results correlating the response of PEI to multiple strain rates.

Finally, have been developed to predict the strain pulse behavior in response to a mSHPB wave shaper, preliminary results are shown in Fig. 31 and Fig. 32, but these models will be modified in order to predict the sensitivity of the apparatus to factors in specimen size, geometry, and interfacial friction.

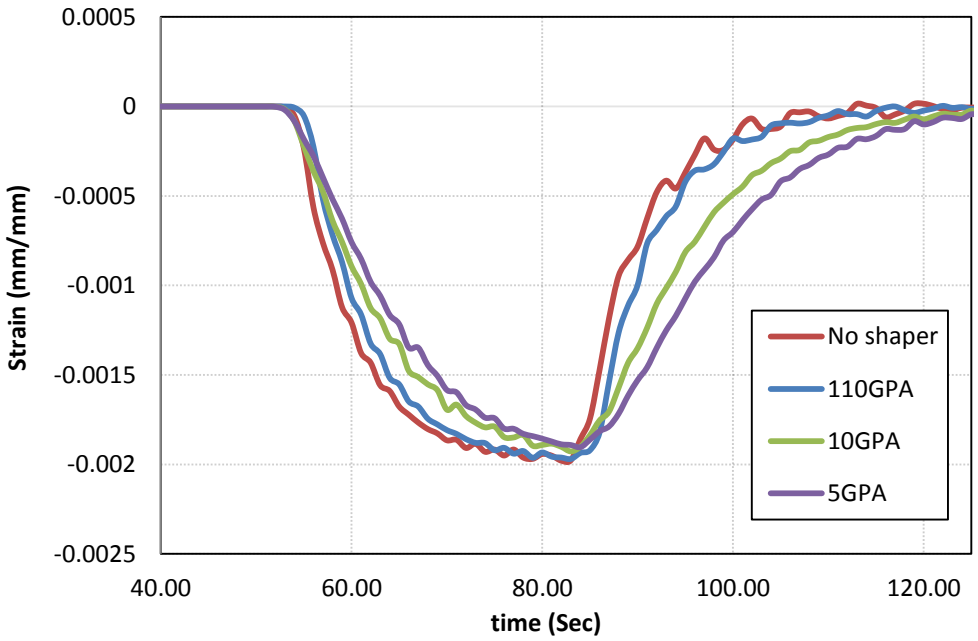

Figure 31. Model predicting the effect of a wave shaper on the mSHPB incident signal.

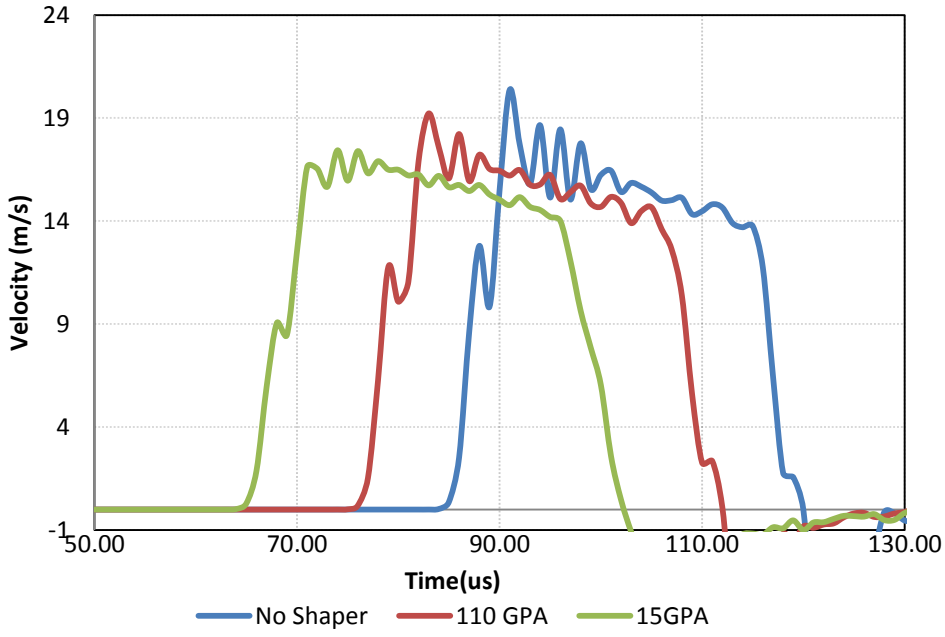

Figure 32. Sensitivity of the peak strain rate in response to a wave shaper of varying stiffness.

APPENDIX A: SUMMARIZED DATA FROM HIGH STRAIN RATE COMPRESSION AND QUASI-STATIC TENSION, TORSION, AND COMPRESSION EXPERIMENTS

Summarized Tensile Response of PEI at room Temperature

Mechanical Properties	Value (English units)	Value (SI units)
Tensile Strength, σ_{ut}	15.5 ksi	107 MPa
Tensile Modulus, E_t	465 ksi	3.2 GPa
Strain at yield, ε_y	7.3 %	7.3%
Strain at break, ε_f	87.3 %	87.3%
Elongation, $EL\%$	80.3%	80.3%
Toughness, U_t	10.8 ksi	74.5 MPa
Upper yield, σ_{uy}	15.5 ksi	107 MPa
Lower Yield, σ_{ly}	12.0 ksi	82.7 MPa
0.02% Yield Strength, σ_{l2}	9.9 ksi	68.3 Mpa
Ramberg-Osgood, α	0.037	0.037
Ramberg-Osgood, n	7.28	7.28

Summarized Compressive Response of PEI at Room Temperature

Mechanical Properties	Value (English units)	Value (SI units)
Compressive Modulus, $\boldsymbol{E_c}$	480 ksi	3.3 GPa
Strain at yield, $\boldsymbol{\varepsilon_{yc}}$	7.2 %	7.2%
Upper yield Strength, $\boldsymbol{\sigma_{uyc}}$	22.4 ksi	154 MPa
Lower Yield Strength, $\boldsymbol{\sigma_{lyc}}$	12 ksi	82.7 MPa
0.02 % Yield Strength, $\boldsymbol{\sigma_{y2}}$	15.5 ksi	106.9 MPa
Ramberg-Osgood, $\boldsymbol{\alpha}$	0.038	0.038
Ramberg-Osgood, *n*	7.53	7.53

Summarized Torsional Response of PEI at Room Temperature

Mechanical Properties	Value (English units)	Value (SI units)
Shear Modulus, G_c	174 ksi	1.20 GPa
Proportional Limit, PL	1.3%	1.3%
Strain at yield, ε_{yt}	15.1 %	15.1%
Shear yield Strength, σ_{sy}	13.96 ksi	96.3 MPa
0.02% Yield Strength	6.2 ksi	42.7 Mpa
Poisson's Ratio, ν	0.362	0.362
Ramberg-Osgood, α	0.0315	0.0315
Ramberg-Osgood, *n*	4.63	4.63

Summarized Compressive Response of PEI at 15,000/s Strain Rate and Room Temperatures

Mechanical Properties	Value (English units)	Value (SI units)
Averaged Elasticity, $\boldsymbol{E_c}$	480 ksi	3.3 GPa
Strain at yield, $\boldsymbol{\varepsilon_{yc}}$	8.5 %	8.5%
Upper yield Strength, $\boldsymbol{\sigma_{uyc}}$	36.1 ksi	248 MPa
Lower Yield Strength, $\boldsymbol{\sigma_{lyc}}$	31 ksi	213 MPa
Material Parameter , $\boldsymbol{A_1, A_2}$	1.70, 1.74 psi/°K	11.7, 12.0 KPa/°K
Activation Energy, $\boldsymbol{Q_1, Q_2}$	70.0, 4.20 kcal/mol	70.0, 4.20 kcal/mol
Material Parameter, $\boldsymbol{C_1, C_2}$	7.00, 35.0 x10^{-7}s	7.00, 35.0 x10^{-7}s

APPENDIX B: LAB VIEW DATA ACQUISITION SYSTEM AND MATLAB DATA PROCESSING ROUTINES.

LabView Data Acquisition Routine for Striker Velocity

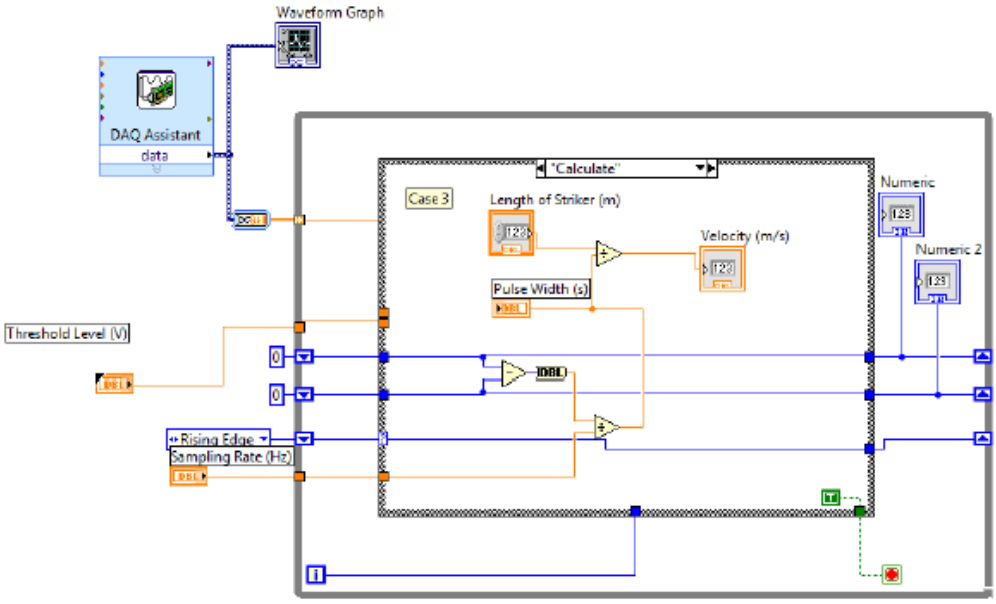

(a)

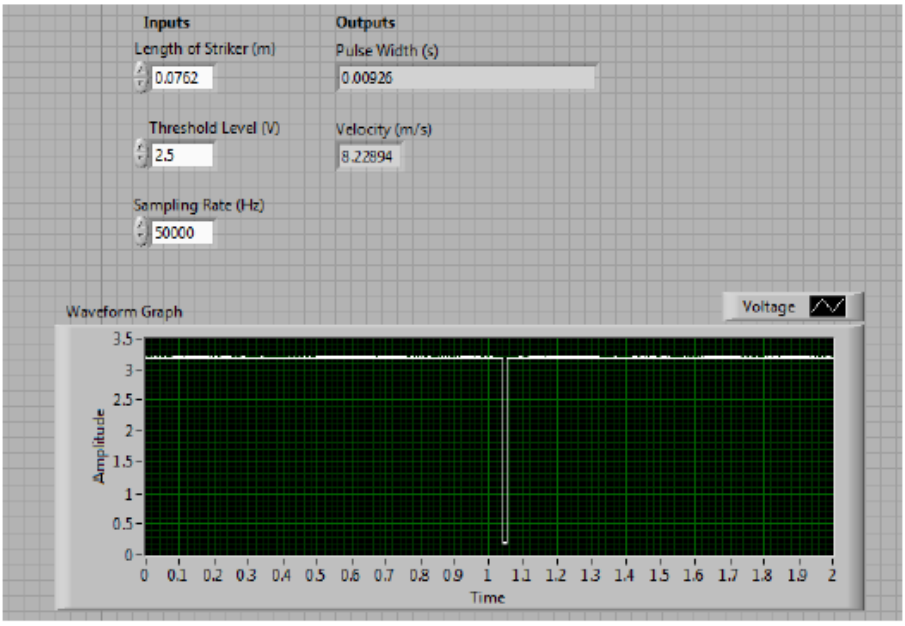

(b)

Matlab Data Processing Routine: Quasi-Static Experiments

```
close all
clc
clear all

%DATA ANALYSIS FOR COMPRESSION/TENSION TESTS
%Bryan Zuanetti

tic

run=4;

%for run=1:6

%Defining Variables
file_name='Test';
pi=2*asin(1);
length=.367;
diameter=.225;
Area=(pi/4)*diameter^2;

%Read time, load, extension and deflection data
time=xlsread(file_name,run,'A2:A723');
Load=xlsread(file_name,run,'B2:B723');
extension=xlsread(file_name,run,'C2:C723');
deflection=xlsread(file_name,run,'D2:D723');

%Define Deflection absolute value
defl_abs=abs(deflection);

%Define Stress and Strain
Stress=Load/(Area*1000);
Strain=defl_abs/length;

%Build Output Matrix
output(:,1)=[defl_abs];
output(:,2)=[Stress];
output(:,3)=[Strain];

%Write Stress, Strain, and deflection
xlswrite(file_name,output,run,'E2:G723');

%Defining Slope and Intercept
y=xlsread(file_name,run,'F1:F200');              %Stress column
```

```
x=xlsread(file_name,run,'G1:G200');              %Strain Column
Start=find(y<5,1,'last');                        %Criteria for
linear portion
Finish=find(y>10,1,'first');                     %of Stress vs
Strain graph
y_new=y(Start:Finish);                           %Choosing the
correct range
x_new=x(Start:Finish);
p = polyfit(x_new,y_new,1);                        %Using Linear
Regression
slope=p(1);                                        %Defining
Slope
y_inter=p(2);                                      %Defining Y
intercept
x_inter=(-y_inter/slope);                          %Defining X
intercept

%Output to screen to check for correctness
fprintf('Slope(MOD),                       :      %6.2f (ksi)\n'
, slope);
fprintf('y_inter,                          :      %6.2f \n'
, y_inter);
fprintf('x_inter,                          :      %6.2f \n'
, x_inter);

%Defining new Strain, and stress
Strain_adj=Strain-x_inter;
Stress_adj=Strain_adj*slope;
Offset=slope*(Strain_adj-.002);
Start2=find(Offset<21,1,'last');
Offset_new=Offset(1:Start2);

%Output and Write New Strain, Stress and Offset
A(:,1)=[Strain_adj];                       %Strain after shift to
origin
A(:,2)=[Stress_adj];                       %Linear Portion of
Stress
Z(:,1)=[Offset_new];                       %.02% percent offset
line
xlswrite(file_name,A,run,'H2:I723');
xlswrite(file_name,Z,run,'J2:J300');

%Finding Yeild Strength
Stress2=Stress(1:Start2);
Offset2=Offset_new;
```

```
Root=Stress2-Offset2;
Zero=Root.^4;
[C,I]=min(Zero);
Yeild_S=Stress2(I);                          %Consider Linearization
for improvement
SUT=max(Stress);
fprintf('Yield_S,                            :      %6.2f (ksi)\n'
, Yeild_S);
fprintf('Tensile_S,                          :      %6.2f (ksi)\n'
, SUT);

%Delete tail portion of Stress and Linearize
[rows,columns]=size(Strain);
c=find(Stress<5,1,'last');
i=1:rows;
for i=1:c
Stress_new(i)=Stress_adj(i);
end
for j=c:rows
    Stress_new(j)=Stress(j);
end
B(:,1)=[Stress_new];
xlswrite(file_name,B,run,'F2:F723');

%make Plot Stress vs Strain
figure;
plot(Strain_adj,Stress_new,'b','LineWidth',3)
grid
title('Stress vs Strain')
legend('Stress')
xlabel('Strain(mm/mm)')
ylabel('Stress(ksi)')

%end

toc
```

Matlab Data Processing Routine: High Strain Rate Experiments

```
close all
clc
clear all

tic
%DATA ANALYSIS FOR MSHB TEST
%Bryan Zuanetti

% Define variables
file_name='Test3';                    % File name
CH1_gain=1208.5;                      % Gain for CH1
CH2_gain=1203.8;                      % Gain for CH2
CH1_intcp=0.0785;                     % Gain intercept for CH1 (V)
CH2_intcp=-0.1742;                    % Gain intercept for CH2 (V)
gauge_factor=2.08;                    % Strain gauge factor
ex_volt=3.288;                        % Bridge excitation voltage
(V)
Cb=4943;                              % Bar wave speed (m/s)
span=101;                             % Smoothing span value (must
be odd)
CH1_cal=1.15;                         % Calibration 1
CH2_cal=1.19;                         % Calibration 2
L0=.001039;
Mod=6.87*(10^10);
Ab=7.92*(10^-6);
As=2.48*(10^-6);
Sample_rate=.00000002;

run=1;

%for run=6:6

% Read time, incident pulse, and transmission pulse vectors
[time]=xlsread(file_name,run,'A14:A16397');
CH1=xlsread(file_name,run,'B14:B16397');
CH2=xlsread(file_name,run,'C14:C16397');


% Reduce magnitude of pulses using gain equation
CH1_gain=(CH1-CH1_intcp)/CH1_gain;
CH2_gain=(CH2-CH2_intcp)/CH2_gain;

% Determine pulse offset zeros
```

```
CH1_zero=mean(CH1_gain(1:500));
CH2_zero=mean(CH2_gain(1:500));

% Offset pulses to start at zero
CH1_adj=CH1_gain-CH1_zero;
CH2_adj=CH2_gain-CH2_zero;


% Convert pulses from voltage to strain
CH1_strain=(4*CH1_adj)/(gauge_factor*ex_volt);
CH2_strain=(4*CH2_adj)/(gauge_factor*ex_volt);

% Calculate theoretical strain pulse amplitude
%amp_theor=(1/2)*(vel/Cb);

% Smooth data
CH1_smooth=smooth(CH1_strain,span,'rlowess');
CH2_smooth=smooth(CH2_strain,span,'rlowess');

% Amplitude Corrected
CH1_Corrected=CH1_smooth*CH1_cal;
CH2_corrected=CH2_smooth*CH2_cal;

% Build matrix of values to write back into excel workbook
output(:,1)=[CH1_gain];
output(:,2)=[CH2_gain];
output(:,3)=[CH1_adj];
output(:,4)=[CH2_adj];
output(:,5)=[CH1_strain];
output(:,6)=[CH2_strain];
output(:,7)=[CH1_smooth];
output(:,8)=[CH2_smooth];
output(:,9)=[CH1_Corrected];
output(:,10)=[CH2_corrected];

% Write output matrix back into excel workbook
xlswrite(file_name,output,run,'D14:M16397');

%Defining Incident, Reflected and transmitted pulse
i=1:16000;
A = CH1_Corrected(i);
C = find(A > .00025);
fprintf('Start,                          :      %6.2f \n'       ,
C(1));
Start=C(1)-300;
```

```
Finish=Start+1750;
%Refinement Process to automatically obtain Incident Pulse
New1=CH1_Corrected(Start:C(1));
C_new=find(New1<.0001,1,'last');
Start_new=C(1)-300+C_new;
Finish_new=Start_new+1750;
Incident_P=CH1_Corrected(Start_new:Finish_new);

D = find(A < -.00025);
fprintf('Start2,                        :      %6.2f \n'       ,
D(1));
Start2=D(1)-300;
Finish2=Start2+1750;
%Refinement Process to automatically obtain Reflected Pulse
New2=CH1_Corrected(Start2:D(1));
D_new=find(New2>-.0001,1,'last');
Start2_new=D(1)-300+D_new;
Finish2_new=Start2_new+1750;
Reflected_P=CH1_Corrected(Start2_new:Finish2_new);

E = CH2_corrected(i);
B = find(E > .00025);
fprintf('Start,                         :      %6.2f \n'       ,
B(1));
Start3=B(1)-300;
Finish3=Start3+1750;
%Refinement Process to automatically obtain Transmitted Pulse
New3=CH2_corrected(Start3:B(1));
B_new=find(New3<.0001,1,'last');
Start3_new=B(1)-300+B_new;
Finish3_new=Start3_new+1750;
Transmitted_P=CH2_corrected(Start3_new:Finish3_new);

%Build output matrix for Incident, Reflected and transmitted
Pulses
OM(:,1)=[Incident_P];
OM(:,2)=[Reflected_P];
OM(:,3)=[Transmitted_P];

%Write Output back into the excel file
xlswrite(file_name,OM,run,'N14:P1764');

%Define Stress, Strain rate, Strain and Strain increment
Strain_Rate=abs((-2*Cb/L0)*Reflected_P);
Stress=abs((Ab/As)*Mod*Transmitted_P)/1000000;
```

```
OM2(:,1)=[Strain_Rate];
OM2(:,2)=[Stress];
Strain_inc=Strain_Rate*Sample_rate;
OM2(:,3)=[Strain_inc];
xlswrite(file_name,OM2,run,'Q14:S1764');


%Defining Strain,creating output and writing on file
[M,O]=size(Incident_P);
N=M+1;
for i=3:N
    Strain(1)=Strain_inc(1);
    Strain(i-1)=Strain(i-2)+Strain_inc(i-1);
end
Strain_rateMPA=Strain_Rate/100;
OM3(:,1)=[Strain];
OM3(:,2)=[Strain_rateMPA];
xlswrite(file_name,OM3,run,'T14:U1764');

%plot Pulse
%figure;
%plot(Incident_P,'b')
%grid
%title('Incident Pulse')
%legend('Trace')
%xlabel('Time')
%ylabel('Incident Pulse(mm/mm)')

%end

toc
```

REFERENCES

1. Ames, N., & Anand, L. (2003). A Theory of Amorphous Polymeric Solids Undergoing Large Deformations: Applications to Micro-indentation of Poly(methyl methacrylate). *Internation Journal of Solids and Structures*, 1465-1487.

2. ASTM Standard, D. (2010). Standard Test Method for Compressive Properties of Rigif Plastics. In A. International, *Annual Book of Standards.*

3. ASTM Standard, D. (2010). Standard Test Method for Tensile Properties of Plastics. In A. International, *Annual Book of Standards.*

4. ASTM Standard, E. (2012). Standard Test Methods for Notched Bar Impact Testing of Metallic Materials. In A. International, *Annual Book of Standards.*

5. ASTM Standard, E.-1. (2010). Standard Practice for Verification and Classification of Extensometer Systems. In A. International, *Annual Book of Standards.*

6. Bansal, A., Jian, K., & Schandler, S. (2002). Mechanical Properties of Polyetherimide-alumina nanocomposites. *SEM Annual Conference and Exposition on Experimental and Applied Mechanics.*

7. Bauwens, C. (1969). Tensile Yield-Stress Bahviour of Glassy Polymers. *Journal of Polymer Science*, 735-742.

8. Beland, S. (1990). High Performance Thermoplastic Resins and Their Composites. 44-45.

9. Bijwe, J. (1990). Friction and Wear Studies of Bulk Polyetherimide. *Journal of Polymer Science*, 548-556.

10. Boyce, M., Socrate, S., & Llana, P. (2000). Constituitive model for the finite deformation stress-strain behavior of Poly(ethyleneterphthalate) above the glass transition. *Journal of Polymer*, 2183-2201.

11. Brown, N., & Ward, I. (1968). Load Drop at Upper Yield Point of Polymer. *Journal of Polymer Science*, 607-620.

12. Charpy, M. (1901). Note Sur l'Essai des Metaux a la Flexion par Choc de Barreau Entailles. *Societe de Ingenierus Francais*, 848.

13. Chen, B., Su, C., Tseng, M., & Tsay, S. (2006). Preparation of Polyetherimide Nanocomposites with Improved Thermal, Mechanical and Dielectric Properties. *Polymer Bulletin*, 671.

14. Chen, e. a. (2006). Preparation of Polyetherimide Nanocomposites with improved Thermal, Mechanical and Dielectric Properties. *Polymer Bulletin*, 671-681.

15. Chen, W., & Song, B. (2011). *Split Hopkinson (kolsky) Bar; Design, Testing, and Applications.* New York: Springer.

16. Chen, W., & Song, B. (2011). Split Hopkinson Bar: Design, Testing and Applications. *mechanical Engineering Series*.

17. Chou, S. (1973). The Effect of Strain Rate and Heat Developed During Deformation on the Stress-Strain Curve of Plastics. *Experimental Mechanics*, 422-432.

18. Chou, S. (1973). The Effect of Strain Rate and Heat Developed During Deformation on the Stress-Strain Curve of Plastics. *Experimental Mechanics*, 422-432.

19. Davies, R. (1948). Critical Study of Hopkinson Pressure Bar. *Royal Society of London*, 376-457.

20. Erying, H. (1936). Viscosity, Plasticity and Diffusion as Examples of Absolute Reaction Rates. *The Journal of Chemical Physics*, 283-291.

21. Facca, A. (2006). Predicting the Elastic Modulus of Hybrid Fibre Reinforced Thermoplastics. *Polymers and Polymer Composites*, 239-250.

22. Garcia, M. e. (2007). Effects of Natural Aging for Eight Years on Static Properties of Glass or Carbon Fibre Reinforced Polyetherimide. *Corrosion Engineering, Science and Technology*, 61-63.

23. Gilat, A. (2000). Torsional Split Hopkinson Bar Tests at Strain Rates Above 10000. *Experimental Mechanics*, 54-59.

24. Gray III, G. (2000). Classic Split-Hopkinson Pressure Bar Testing. *ASM Handbook 8 Mechnical Testing and Evaluation*, 463-476.

25. Gray III, G., & Blumenthal, W. (2000). Split-Hopkinson Pressure Bar Testing of Soft Materials. In A. H. 8, *Mechanical Testing and Evaluation* (pp. 488-496).

26. Gray, G., Blumenthal, w., Trujil, C., & Carpenter, R. (1977). Influence of temperature and Strain Rate on the Mechanical Behavior of Adiprene L-100. *Journal de Physique*, 523-528.

27. Harding, J. (1960). Tensile Testing of Materials at Impact Rates of Strain. *Journal of Mechanical Engineering Science*, 88-96.

28. Hopkinson, B. (1914). A method of Measuring the Pressure Produced in the Detonation of High Expolosives or by Impact of Bullets. *Philosophical Transactions of the royal Society of London*, 19.

29. Jia, D. (2004). A rigrous Assessment of the Benefits of Miniaturization in the Kolsky Bar System. *Experimental Mechanics*, 445-454.

30. Jordan, J. F. (2008). Mechanical Properties of EPon 826/DEA Epoxy. *Mechanics of Time-Dependent Materials*, 249-272.

31. Kierkels, J. (2006). Tailring the Mechanical Properites of Amorphous Polymers. *Technische University of Eindhoven*.

32. Kolsky, H. (1949). An investigation of the Mechanical Properties of Materials at Very High Strain Rates of Loading. *proceedings of the Physical Society*, 676-700.

33. Mahajan, D., Estevez, R., & Basu, S. (2010). Ageing and rejuvenation in Glassy Amorphous Polymers. *Journal of the Mechanics and Physics of Solids*, 1474-1488.

34. Marano, C., & Rink, M. (2013). Viscoelasticity and Shear Yielding Onset in Amorphous Glassy Polymers. *Mechanics of Time-dependent Materials*, 173-184.

35. Mulliken, A. (2006). Mechanics of Amorphous Polymers and Polymer Nanocomposites During High Rate Deformation. *PHD Thesis, Mechanical Engineering, MIT*.

36. Mutter, N. (2010). Characterization of Dynamics and Static Behavior of Polyetherimide. *Master's Thesis, University of Central Florida*.

37. Nemat-Nasser, S., Isaacs, j., & Rome, J. (2000). Triazial Hopkinson Techniques. In A. International, *ASM Handbook Volume 8 Mechanical Testing and Evaluations* (pp. 516-518).

38. Pecht, M. (1994). Characterization of Polyimides Used in Ge High Density Interconnects. *7th International SAMPE Electronics Conference*, (pp. 432-445).

39. Prakash, V., & Mehta, N. (2012). Uniaxial Compression and Combined Compression and Shear Response of Amorphous Polycarbonate at High Loading Rates. *Polymer Engineering and Science*, 1217-1231.

40. Ree, T. (1955). Theory of Non-Newtonian Flow Solutions Sytems of High Polymers. *Journal of Applied Physics*, 800-809.

41. Roetling, J. (1965). Yield Stress Behavior of Poly(ethyl methacrylate) in the glass transition region. *Journal of Polymers*, 615-619.

42. Russel, S. (1898). Experiments with a New Machine for Testing Materials by Impact. *Transactions ASCE*, 237-250.

43. Schossig, S., Bierogel, C., & Grellman, W. (2008). Mechanical Behavior of Glass-fiber reinforced thermoplastics materials under high strain rates. *Polymer Testing*, 893-900.

44. Simon, S., Plazek, D., Sobieski, J., & McGregor, E. (1996). Physical Aging of a Polyetherimide: Volume Recovery and its comparison to creep and enthalpy measurements. *Journal of Polymer Science Part B-Polymer Physics*, 929-936.

45. Siviour, R. (2005). The High Strain Rate Compressive Behavior of Polycarbonate and Polyvinylidene Difluoride. *Polymer*, 1246-1255.

46. Smmazcelik, T. (1991). Impact-fatigue Behaviour of Uniderectional Carbon Fibre Reinforced Polyetherimide (PEI) Composites. *Journal of Material Science*, 6237-6244.

47. Struik, L. (1978). Physical Aging in Amorphous Polymers and Other Materials. *Elsevier Scientif Publication Corporation*.

48. Swallowe, G. (1999). Mechanical Properties and Testing of Polymers. *Kluwer Academic*.

49. Vina, J., Castrillo, M., Arguelles, A., & Vina, I. (2002). A Comparison between the Static and Fatigue Properties of Galss-fibre and Carbon-fibre Reinforced Polyetherimide Composites after Prolonged Aging. *Journal of Polymer Composites*, 619-623.

50. Voce, E. (1948). The relationship between Stress and Strain for Homogenous Deformation. *Journal Institute Metallurgia*, 537-562.

51. Voce, E. (1955). A Practical Strain Hardening Function. *Journal Institute Metallurgia*, 219-226.

52. Walley, S. (1989). A study of the Rapid Deformation Behaviour of a Range of Polymers. *Philosophical Transactions of the Royal Society of London*, 1-33.

53. Walley, S. (1991). A Comparison of the High Strain Rate Behaviour in Compression of Polymers at 300 K and 100 K. *Journal de Physique*, 185-195.

54. Walley, S. (1991). The Rapid Deformation of Various Polymers. *Journal de Physique*, 1889-1925.

55. Zhou, C., Vaccaro, N., Sundarram, S., & Li, W. (2012). Fabrication and Characterization of Polyetherimide Nanofoams Using Supercritical CO2. *Journal of Cellular Plastics*, 239-255.